SIZE FOCUSING APPROACH OF HIGH CONCENTRATION $CU_{2-X}S$ NANOPARTICLES

AND SCALABLE SYNTHESIS METHODOLOGY OF PURE PHASE COPPER TIN SULPHIDE

A Thesis

Presented to the Faculty of the Graduate School

of Cornell University

In Partial Fulfillment of the Requirements for the Degree of

Master of Science

by

Shinjini Biswas

August 2018

ABSTRACT

"There is plenty of room at the bottom" – Richard Feynman (1959)

Nanoparticles and their size dependent properties have long since revolutionized the technological industry from the way engineers conceptualize and design modern devices to the way scientists understand the underlying physics and its potential implications. Intricate control on the sizes of semiconductor nanoparticles results in profound control over the bandgap making absorptions and emissions increasingly efficient. However, synthesis of scalable amounts of size focused nanoparticles remain the biggest challenge in the industry. A polydisperse distribution of sizes corresponds to a variation in its properties which nullifies the primary motivation of using nanoparticles. Moreover, for nanoparticles to become a standing competitor in the semiconductor industry, there is a need to establish synthesis procedures compatible with scalable large-scale nanoparticle manufacturing without undermining their crucial dimensional influence. These procedures are prey to a wide variety of parameters starting from the preliminary salts, their chemical interactions to physical stimulus making optimization of each material on a large scale all the more difficult. We substantiate this need with a nanoparticle reusability concept wherein any batch of polydisperse particles can be transformed to a size tuned group with the help of an etchant (Oleylamine or Chlorine) and re-grown with heat-up technique. This post synthesis treatment enables the use of large scale synthesized particles and tune their sizes corresponding to the desired application. In this thesis we were successful in tuning the size to 8.5nm with a dispersity of 7%. The etchant is used to decrease the size variation in the polydisperse batch and produce monomers. Monomer saturations in turn combat competitive growth or Ostwald ripening and instead help the larger particles to grow uniformly when heated up. Our investigations are heavily concentrated in the $Cu_{2-x}S$ system which is viewed as a practical substituent to other toxic counterparts like

Cadmium or lead based semiconductor nanoparticles. Understanding this system forms a conceptual foundation for manipulating related ternary and quaternary compounds like Copper-Indium-Sulphide(CIS) or Copper-Tin-Sulphide(CTS) which have a host of applications of their own. We also elucidate a method of utilizing high concentration scalable production to create phase pure batches of Mohite CTS. These particles exhibit band gaps ranging from 1.04eV to 1.38eV which is suitable to most opto-electronic applications like solar cells and photodetectors. Future work would be to extend the particle reusability to other systems, investigate influence on associated ternary and quaternary compounds thus probing a step closer in making this approach acceptable commercially. Furthermore, creating devices from these size tuned particles and reviewing any improvements would exhibit great progress in the study of copper-chalcogenide nanoparticles and their potential in the industry.

BIOGRAPHICAL SKETCH

The author of this Masters of Science Thesis is Shinjini Biswas. She had been pursuing Masters of Science in the Department of Materials Science and Engineering at Cornell University from 2016 to 2018. She had procured her Bachelors of Science Research (BSc. Research) from the Materials Science and Engineering Department at Indian Institute of Science, Bangalore (2012-2016)

ACKNOWLEDGMENTS

I would like to extend deep gratitude towards my MS Committee comprising of Prof. Richard D. Robinson and Prof. Tobias Hanrath for their supervision and guidance throughout my research and professional endeavors. Their scientific insight and professional advice has not only broadened my mind but also improved my scientific perception. I would like to acknowledge the Cornell University, the MSE department and CCMR for allowing me access to facilities for materials characterization and for giving me this opportunity to pursue research in nanomaterials. My research was sponsored by the National Science Foundation (NSF) under the award number CMMI-1344562. I would like to extend my thanks to my fellow lab mates Dough Nevers, Curtis Williamson, Andrew Nelson, Anuj Bharadwaj, Johnathan Neff and Zhiqi Wang for their fresh scientific insight, collaborations, and analytical ideas without which I could never have completed my research successfully. Lastly, I owe all my work and achievements to my family and friends for their consistent support and encouragement without whom none of this would be possible.

TABLE OF CONTENTS

CHAPTER 1

SIZE FOCUSING OF HIGH CONCENTRATION $CU_{2-X}S$ NANOPARTICLES BY CONTROLLED ETCHING AND GROWTH

Shinjini Biswas, Dough Nevers, Curtis Williamson, and Richard Robinson
– Work to be published

Abstract

Size focusing continues to be a difficult challenge in the field of nano-particle synthesis due to rampant Ostwald ripening of growing nano-particles. It is crucial that we achieve size tuned particles in turn attaining mono-dispersity in order to realize the size dependent properties of the nanoparticles in its full potential. We report a novel synthesis method in which we use pre-made Copper Sulphide seeds which we size focus into a monodisperse set of nano-particles (8.5nm). NP growth is controlled via tuning the etch strength of the solution environment. Specifically, increasing the OLA concentration strongly enhances the etching of NP seeds, and upon growth yields more monodisperse particles (7% dispersity). The strength of OLA etch can be mitigated and tuned with the addition of chlorine ions. Control over the degree of etching enables control over the monomer (*i.e.* etch material) concentration in the solution. Re-growing these particles in a monomer saturated solution helps reduce Ostwald ripening effects to yield mono-dispersity in the newly formed nanoparticles. This work not only reports the impact of

tuning etch strength of the solution in achieving size focusing but also suggests reusability of nanoparticles to form new ones of desired size and dispersity.

1.1 Introduction

Size dependent properties of nanoparticles is the highlight characteristic that has the potential to enable advances in the development of opto-electronic devices [1-4]. Its impact is realized especially in light harvesting applications like photovoltaics [5-7] and photodetectors [8-11], light-emitting applications like LEDs [12-15], in energy storage devices like fuel cells [16] and a host of biological purposes [17]. To ensure that the potential of the nanoparticles is realized, efforts have been made to synthesize particles with a narrow size distribution [18] focused at the desired sizes. Maintaining monodispersity is of vital importance for facilitating inorganic colloid assembly into superlattices [19] and developing long range ordered solids revealing excitonic bands [20].

$Cu_{2-x}S$ is a p-type semiconductor that is emerging as a good substituent material to current cadmium-based or lead-based semiconductors due to its non-toxic nature. $Cu_{2-x}S$ is a material that exhibits plasmonic properties[21-23] that can be tuned by varying the stoichiometry which is easily achievable by incorporating copper vacancies. In addition, the $Cu_{2-x}S$ system provides a firm foundation for creation of optically active materials often as a copper-metal-sulfide e.g. Copper-Indium-Sulfides [24] or quaternaries like Copper-Zinc-Tin-Sulfides[9] or copper-indium-zinc-sulfides [25]. Thus, understanding how to manipulate the sizes for this system allows us to indirectly have control over the production of other related systems and impact multiple projects related to those particles.

The primary goals in any nanomaterial synthesis that aims to be commercially successful is to have a low size dispersion to maintain its size dependent properties and to be easily scaled up. Most synthesis procedures used to make nanoparticles today rely on hot-injection method of synthesis which shows 5-10% size dispersion [26][27]. However, this method is dependent on multiple parameters making large scale manufacturing very difficult. Also, the process needs to be re-designed and optimized for every new system. Our group, in a previous paper developed a novel process design which utilized the heat up method for achieving scalable nanomanufacturing of various nanomaterials [28]. We build on this foundation of high concentration synthesis technique and further suggest a way to size-focus to any size and obtain mono-dispersity in these particles after synthesis. Here instead of starting from monomer salts which demands optimization of the reaction for each material, we indicate a way to reuse pre-synthesized polydisperse batches of particles thus saving resources and time spent for research efforts while complimenting scalable nanomanufacturing. Extrapolation of our idea would be large scale production of nanoparticles without worrying about its dispersity and in a post synthesis treatment tune the size of the particles to be suited for the desired applications.

Our solution to this growing need is to present a way to use synthesized polydisperse nanoparticles and size focus them according to the desired application. Here we compliment the production technique of high concentration nanoparticle synthesis with a post synthesis treatment for the particles. This involves the nanoparticles produced in large batches to be taken in a solution containing excessive Oleylamine (OLA) and grow them in the same solution by simply heating it up. The use of OLA in nanoparticle synthesis until now has been primarily as a passivating agent, reducing agent or a surfactant[29-31]. The work reported recently by Zamikov

have depicted a similar way of using ligands to control size growth [32], however, in our study we show for the first time that when OLA is present in excess it has an etching effect on the particles.

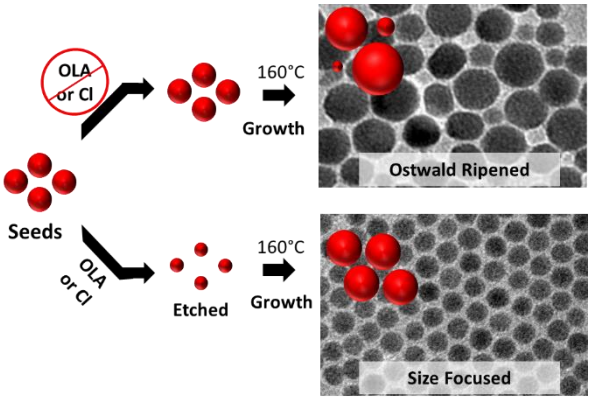

Figure 1.1. *Post-synthesis treatment of pre-synthesized nanoparticles (seeds):* upper path shows nanoparticle growth in a solution devoid of any etchant exhibiting Ostwald ripening; lower path shows nanoparticle growth in solution with etchant revealing size focused growth.

The influence that this unique nature of OLA has on the particles' growth is shown in **Figure 1.1**. Here we see that when the pre-synthesized particles are grown in a solution devoid of any etchant they yield sizes with a large variation mostly due to Ostwald ripening of the particles. This competitive growth is a great struggle to overcome in nano-particle synthesis and efforts of varied nature have been used to combat it. Utilizing the etchant, we were able to control the dispersity of the particles as shown in the lower path in the **Figure 1.1** schematic. Our work aims to provide a plausible concept of reusability where simply controlling the balance of etching and regrowth time of the particles in the solution can realize any-size to any-size transformation in nanoparticles without having to resort to synthesis from salt monomers and eliminating many dependences on environmental parameters.

1.2 Materials

The following chemicals were used as received: Oleylamine (OLA, 98% primary amines), 1-octadecene (ODE, 90%), Copper(I) chloride (97%), and elemental sulfur (purified by sublimation, particle size~100 mesh) were purchased from Sigma-Aldrich. Hexanes (BDH ACS Grade) and ethanol (Ethanol, 200 proof, Anhydrous KOPTEC USP) were purchased from VMR International.

1.3 Experimental Procedures

Synthesis of 4nm $Cu_{2-x}S$ seeds –

1 g of CuCl is mixed with 7 ml of Oleylamine (OLA) and 3ml of 1-Octadectene (ODE) in a round bottom flask. The mixture is degassed and heated up to 110 °C under vacuum, where it is allowed to mix for 2 hours until the solution becomes a tan color. The CuCl solution is then cooled down to 50 °C and put under nitrogen. In a separate round bottom flask 1.6 g of Sulfur is mixed with 7 ml of OLA and 3 ml of ODE. The mixture is degassed and put under nitrogen before heating it up to 110 °C where it is allowed to mix for 1 hour. The solution is then cooled down to 50 °C and 1 ml of this sulfur solution is taken and added to the CuCl solution also at 50 °C. The solution is stirred for 10 mins and is then brought to room temperature which is poured out into centrifuge tubes with excess of ethanol. The product is then centrifuged for 5 min at 4400 rotations per minute. Then the solution is washed 3 times by resuspending in hexane, precipitating by ethanol and centrifuging as done earlier.

Synthesis of 9nm $Cu_{2-x}S$ seeds –

Same preparation steps as when synthesizing 4 nm seeds were taken for dissolving CuCl and Sulfur. Once the CuCl and the Sulfur solutions are prepared separately 1 ml of the Sulfur solution is added to the CuCl solution. The mixture is heated to 180 °C where it is soaked for 2 hours after which it is quenched to room temperature. The particles are precipitated out of the solution and cleaned by the same procedure as stated in the synthesis of 4 nm seeds.

Etching of seeds procedure –

The cleaned seeds (either 4 nm or 9 nm) are weighed and mixed into solutions of varying OLA: ODE ratios (only OLA, 7:3 OLA: ODE, 3:7 OLA: ODE, only ODE). The mixture is degassed and stirred at room temperature for varying amounts of time (10 mins, 30 mins, 1 hour, 2 hour). The seeds are then crashed out of the solution by adding excess of ethanol and centrifuged. The same cleaning procedure as for the synthesis was followed.

Regrowth of etched seeds –

After the premade 4 nm particles are washed and cleaned they are mixed with either an etch promoting solution i.e. one with only OLA ligands or etch preventing solution i.e. with only ODE. After mixing for 20 mins, such that the solution attains its maximum monomer saturation limit, the temperature is ramped up to 160 °C to initiate growth. The particles are left at the temperature for 2 hours before being cooled down, cleaned and dried.

Characterization methods –

X-ray powder diffraction (XRD) data were collected on a Bruker D8 General Area Detector Diffraction System (Cu Kα radiation, ~ 1.54 Å). Samples were washed with ethanol,

centrifuged, and resuspend in hexane three times. After the three wash, the samples were dried overnight before XRD analysis.

Transmission electron microscopy (TEM) analysis was performed on FEI Tecnai T12 transmission electron microscope operating at 120 kV with a LaB6 tip. Samples for TEM analysis were prepared by placing a drop of NP solution in toluene on top of a copper grid coated with an amorphous carbon film. Particle counting was done manually using ImageJ (0.33 nm/pixel resolution). A 100-nanoparticle count was used to measure average size and relative size distribution.

1.4 Results and Discussions

Minimizing nanoparticle size dispersion focuses predominantly on controlling the mechanics of particle growth, changes in chemical environment, pressure, and temperature. We concentrate our efforts in controlling the chemical environment to tune the degree of deposition, etching, and passivation at the nanoparticle surface. By using purified nanoparticle seeds and controlling the solution environment, we can more precisely elucidate the impact of different chemical environments on nanoparticle growth.

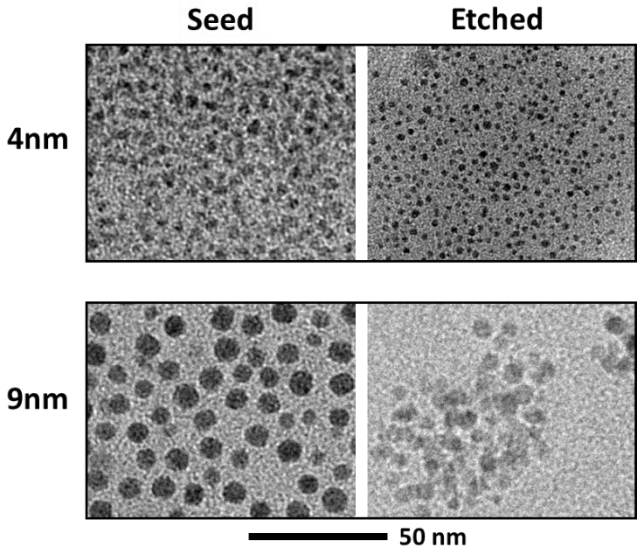

Figure 1.2. *TEM images showing seeds before and after etching for 10 mins in OLA at room temperature showing a considerable decrease in particle size*. (Top left) 4nm seeds before etching; (Top right) 9nm crystalline seeds before etching; (Bottom left) 4nm seeds after etching in OLA showing reduced size; (Bottom right) 9nm seeds after etching in OLA showing reduced size.

We use pre-synthesized $Cu_{2-x}S$ nanoparticle seeds based on a high concentration method [1] as the starting material, owing to their high yields and production. The synthesized 4nm seeds are cleaned thoroughly by redispersion in hexane and ethanol. To probe the effect of solution environment on cleaned NPs, we resuspend 4 nm seeds and 9 nm nanoparticles in pure OLA (**Figure 1.2** left). After resuspension, we observe a decrease in particles size. The 4nm seeds shrunk to 2nm, whereas the 9 nm nanoparticles decrease to 5nm (**Figure 1.2**). This decrease in size indicates dissolution of the particle. The TEM images (**Figure 1.2**) demonstrates that the nanoparticles are being etched when mixed in OLA even when the seeds are completely crystalline. The etching process is relevant for all particle sizes, as both the minuscule (3-4nm) seeds and the large nanoparticles show a decreased size.

To confirm the etching effect of the OLA on the seeds we quantify the dissolution of the particles in terms of the etched mass percent, based on the initial mass of seeds, for a variety of OLA: ODE ratios (**Figure 1.3**). Mixing 4nm seeds in pure OLA solution results in a 65% decrease in the mass of the seeds compared to the initially loaded mass. Based on replicate experiments, we observe that the loss in mass is consistent within 5% over 3 trials. A control experiment was done by simply rewashing and drying the seeds before recording their new weight, in order to identify if there is any loss of seed mass due to cleaning procedures alone. The results for this experiment for deducing the losses due to washing of the seeds, showed an average loss of 10% confirming that the difference in mass recorded before and after the seeds are exposed to OLA was not due to loss of particles when cleaning the seeds but due to interaction with the OLA ligands and in turn etching. We investigate the impact of OLA on etching the nanoparticles by varying its concentration, diluted by ODE. The seeds were mixed in solutions with OLA: ODE ratios of 1:0, 3:7, 7:3, and 0:1. We observe that with increasing OLA: ODE ratio the etched percentage increases linearly from 10% with no OLA to 65% with pure OLA which suggests that in the 10 mins of exposure to the solution this etching effect is stronger when the ligands are present in increasing concentrations (**Figure 1.3** black line). The loss of mass for the only ODE solution is within the noise of our cleaning procedure (10% mass loss) and can be considered a "no etch" or "Stable" condition. The lack of etching in ODE is expected based on its noncoordinating nature [33], whereas, the strong etching of OLA has not been previously observed.

XRD plots of seeds after exposure to the solutions with varying ratios of OLA is depicted in **Figures S1, S2 and S3.** Here we see that the phase of the Copper Sulphide particles remain as Roxbyite and no phase change is seen due to progressive etching.

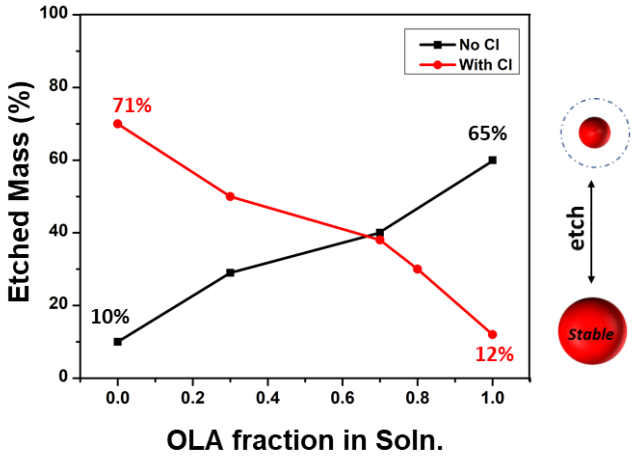

Figure 1.3. *Etched mass from nanoparticle seeds:* The mass percent lost from seeds after etching and wash procedures relative to the starting amount. The black trend shows a clear increase in mass % lost as OLA concentration is increased confirming etching. The red trend shows a similar loss of mass when Chlorine is present but with decreasing concentration of OLA.

Previous $Cu_{2-x}S$ synthesis by our group optimized for scale up nano-manufacturing of the particles, use CuCl as the metal precursor for their particles, and hence Chlorine would also be present in the solution. To probe the effect on nanoparticles from the presence of Chlorine in the solution, we repeat our experiment of resuspending the seeds in solutions of OLA: ODE, but also introduced 1M eq. of Cl ions in the form of HCl. Surprisingly, the addition of chlorine ions leads to a decrease in the etched mass as OLA ligands increased in the solution. (**Figure 1.3** red curve). In the case of only ODE + Cl ions, we observe a drastic loss of mass, which indicates that the seeds are being etches the seeds. However, as we increase the concentration of OLA in the solution, maintaining a 1M eq. of Cl ions, there is a consistent decrease in the

etched mass percent. In a solution with only OLA + Cl ions, mass is recovered (12% etched); in contrast to, 35% recovery for OLA without Cl; Hence, while both OLA and Cl are etchants independently, together they deactivate, hindering the etch process and enhancing colloidal stability of the solution. The two states of the particle i.e. etched or stable are inferred to be interchangable and is depicted in a small schematic adjascent to the plot.

To further quantify the stabilizing effect of Chlorine, we analyzed the mass before and after mixing the 4nm seeds in solutions of various OLA: Cl ratios in ODE. **Figure 1.4** shows the amount of mass retained as seeds after suspending in solution. We used a variety of Cl and OLA ratios. We deduce from the data that at the molar ratio of 3:1 OLA: -Cl there is minimum to no loss of seed mass, indicating that there is no etching of the seeds. The mass yield % are tabulated in **Table 2** in the Supporting Information. Maintaining this ratio of 3:1 OLA: -Cl across different ratios of OLA: ODE shows that a high yield can be maintained even in solutions which without the presence of Chlorine promotes etching of the seeds. We conclude from this study that the colloidal stability of the seed solution can be disrupted using etchants or maintained using coordinating etchants (i.e. amines and halides).

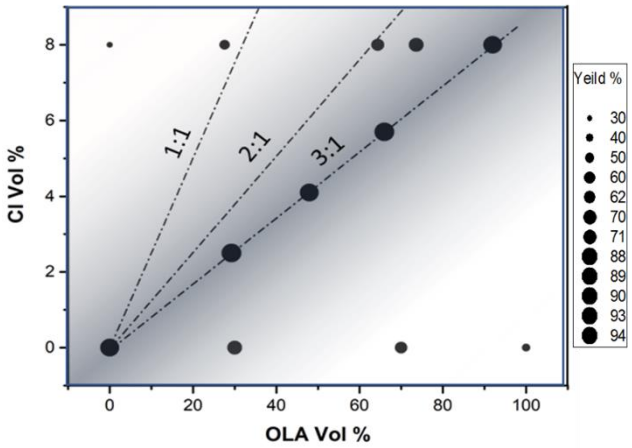

Figure 1.4. Bubble plot of seed mass retained after etching in solutions of different Chlorine and OLA volume %. A 3:1 OLA:Cl ratio corresponds to consistent maintenance of high yield as shown by the large bubbles.

We delve deeper into the evolution of the OLA promoted etching with time by mixing the particles in solutions of varying OLA concentrations for different durations (10mins, 30mins, 60mins, 2hrs). **Figure 1.5a** shows this time resolved yield experiment and is described using a copper monomer concentration for a variety of OLA concentrations where the monomer concentration rapidly decreases initially in all case, and then close stability at an equilibrium or saturation value. The copper monomer concentration is determined from the mass loss measured for each experiment. In the first 10 minutes the seeds or the particles show etching and if the seeds are allowed to mix in the solution for extended amount of time, continued etching is observed until the saturation condition is reached. The seed mass recovered after exposed to the etching solution initially decrease, but then level off at a particular value. After leveling off, the yields unchanged by additional exposure to the etched solution. We can use this mass of seeds retained to back calculate out the concentration of monomers that can be produced due to etching at any given moment of time. The calculation is shown in the SI and it is assumed that all of the mass lost is due to the seeds being etched into monomers which are lost in the supernatant while cleaning. The monomer concentration at saturation levels are indicated for each condition with the help of a solid line. (value and uncertainties in **Table S1** along with Sulphur monomer concentration). With increasing concentration of OLA or in other words more etch prone solutions the supernatant when crashing out seeds are observed to be progressively darker green hence confirming the increased presence of Copper ions.

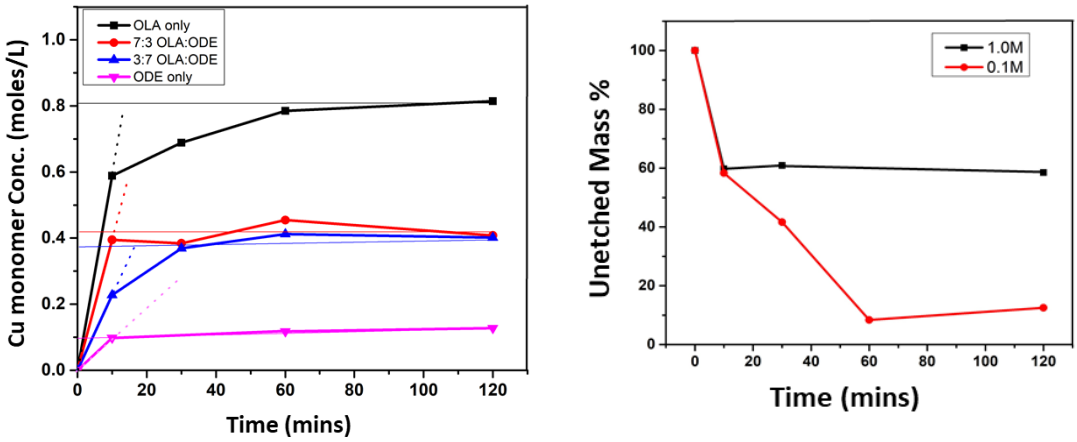

Figure 1.5. *Time resolve etch trends of seeds at room temperature*: **a)** The change in copper monomer concentration in solution with time when etching the seeds in solutions with varying OLA: ODE ratios. (Black – OLA only; Red – 7:3 OLA: ODE; Blue – 3:7 OLA: ODE; pink – ODE only) The saturation values are shown with dashed lines for each trend and dotted lines indicate the etch rates of each solution. **b)** The mass % of unetched seeds after etching different initial seed concentrations (Red – 0.1M and Black - 1M) in 7:3 OLA: ODE solution.

Figure 1.5b. is a plot of seed mass retained when we started with different seed concentrations 0.1M eq and1M eq. to a 7:3 OLA: ODE solution at room temperature and allowed it to mix for different time spans. This data shows a similar plateauing of the maximum seed that can be retained. We observe that when we start with a dilute seed concentration (0.1 M eq.) the etch rate is qualitatively faster in the first 10 mins than that that seen in higher concentrations. Increasing the concentration to 1M or very high concentration regime shows a lower rate of etch in the first 10 mins and more time to achieve a monomer saturation value. These etch rates, which are depicted by the dotted lines, are estimated from the first 10 mins of the mixing as after that time the seed mass plateaus. This observation suggests that as the amount of seeds are

increased with respect to the OLA, the etching effect that the OLA has on the seed surface is delayed. In the dilute cases there is a surplus of OLA present which is able to interact with the surface and etch away copper ions and achieve monomer saturation faster, whereas the more concentrated the solution is with seeds there is fewer OLA ligands (by a factor of 20) per seed and hence this etching effect is decreased, and it takes more amount of time to achieve a monomer saturation.

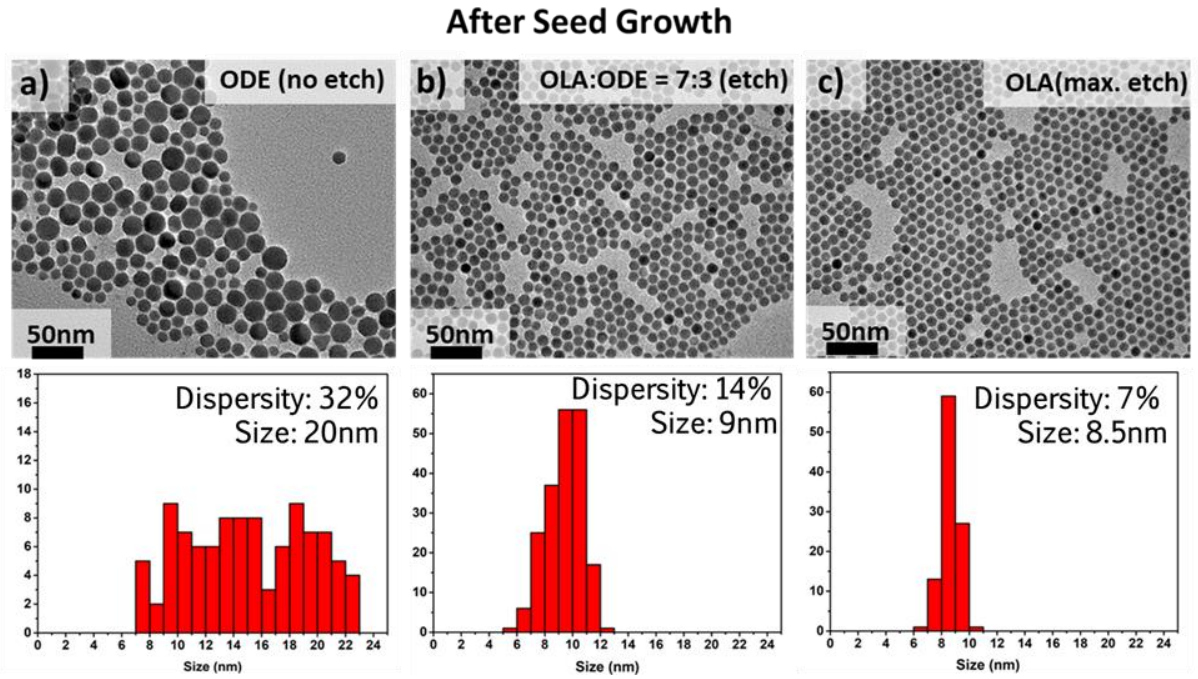

Figure 1.6. The TEM of the regrown seeds, and histograms displaying the effect of etching conditions on the resulting dispersity of the particles. **a)** The seeds in pure ODE (zero etching condition) grow into large particle size (20nm) and dispersity of 32%. **b)** The seeds in OLA: ODE 7:3 solution (i.e. intermediate etching conditions) grow into smaller and more uniform particles: size (9nm) and dispersity of 14%. **c)** The seeds in pure OLA (highest etching conditions) are similar to the 7:3 OLA: ODE case, but show the enhanced size focusing (8.5nm) and a dispersity of 7%.

To understand how these etching conditions, contribute to the seed's subsequent growth, we re-grew the seeds in the different solutions and compared the resulting particles. **Figure 1.6** shows the TEM images of the seeds after regrowth in solutions of varying OLA concentrations along with a histogram plot of the resultant particle sizes. Based on this analysis, we observe that both the average size and the spread of the full width half max (FWHM) decrease as the solution increases in OLA concentration. In **Figure 1.6a,** the particles are in a non-etching or colloidally stable environment (ODE) which show a significant growth of particle size reaching up to 21nm and substantially size dispersion (~ 32%). **Figure 1.6b**, shows an intermediate stage where the seeds were regrown in 7:3 OLA: ODE ratio. Compared to those grown in ODE, this result shows a large (factor of 2) decrease in the dispersity (14%) and significantly size focused to 9 nm nanoparticles. In **Figure 1.6c**. we observe that in the solution containing only OLA ligands, thus extremely etch promoting, the nanoparticles size focus further to 8.5 nm with a factor of 2 lower dispersity (7%) compared to the 7:3 OLA: ODE case. The narrowing spread of distribution is clear in the histograms, which show increasingly more focused nanoparticles with increasing OLA. The regrowth experiment together with the OLA etching study (i.e., the increased copper monomer concentrations with increased OLA concentration) support the conclusion that increasing in the monomer concentrations prior to growth promotes enhanced size focusing.

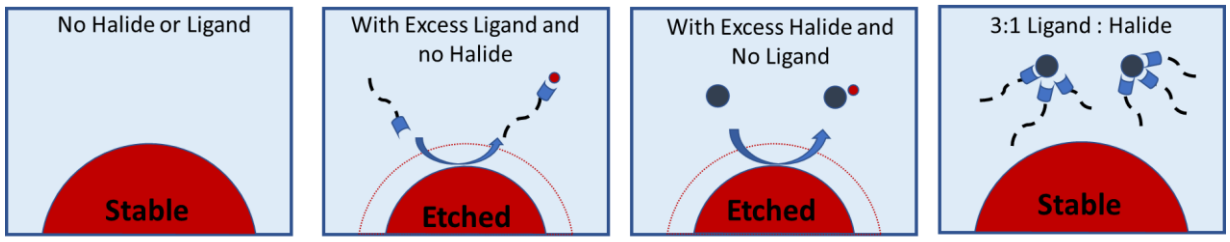

Figure 1.7. The concept of etching and stabilizing of NPs or seeds at room temperature. a) particles in a solution devoid of etchants are stable b) Particles in a solution with OLA ligands in excess showing etching c) Particles in a solution with Chlorine ions in excess shows etching d) Particles in a solution of 3:1 OLA: -Cl shows no etching and complexing of etchants.

Mechanistically, these results indicate that nanoparticle seeds and their subsequent growth are highly sensitive to their solution environment. The seeds are stable in non-interacting (i.e. noncoordinating) solutions such as ODE (**Figure 1.7a**). Hence, this no-etch condition produces no monomers and upon regrowth the seeds interact with other seeds (rather than monomer), yielding Ostwald ripening where bigger particles grow bigger at the expense of smaller ones. This ripening-based growth causes large dispersion in the seed sizes as seen in **Figure 1.6a**. As the amount of coordinating OLA ligands are increased in the solution, the ligands interact with the surface of the seeds. They react with the Copper and Sulphur on the surface of the particle, complexing with them and pulling them into solution (**Figure 1.7b**). This etched species referred to as monomers are ready to aid the growth of the remaining nanoparticles when desirable growth conditions are met (increasing temperatures). This is the key to reducing the effects of Ostwald ripening and achieving size focused nanoparticles. We are not limited by the dispersity of size in the starting seeds but upon etching we stabilize the sizes of the particles and allow uniform growth of the nano-particles. In addition, the more OLA ligands are present in the solution compared to the seeds the higher the monomer concentration in the solution due

to etching is achieved because more ligands can react simultaneously with the seed. The dotted red circle around the seeds show the original size of the seeds and display how the seed has shrunk on being etched by the ligands.

Revisiting our discussion about the effects on the seed when Chlorine ions are present in the solution, we observed that when the OLA: Cl is balanced to 3:1 in each case of varying OLA concentrations in the solution, explained by consistently seeing a high seed mass retention of around 90%. The values are tabulated in **SI (Table 2)**. In other cases where there are halides present in the solution with minimal to no ligands the particle etches and there is a loss of mass indicating that chlorine also exhibits etching characteristics which is illustrated in **Figure 1.7c**. However, we can speculate that at 3:1 OLA: -Cl ratio, the chlorine interacts with the OLA ligands to form a complex therefore protecting the seeds from being etched by either, making the particle stable (**Figure 1.7d)**. This gives us an additional method to control the colloidal stability of any solution of OLA and ODE.

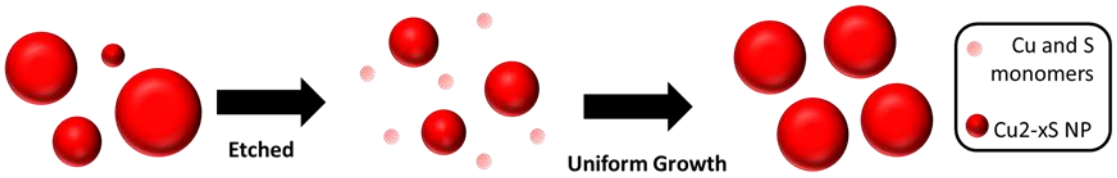

Figure 1.8. *Etch mediated growth mechanism to produce monodisperse nano-particles.* The polydisperse set of particles when etched form monomers and particles of reduced size difference. When these particles are grown in situ the monomers aid in uniform growth into monodisperse particles and inhibit Ostwald ripening

The growth of the particles after etching can be visualized by the schematic in **Figure 1.8**. We started with a polydisperse batch of particles. Upon etching in suitable etching solutions, the smaller particles disintegrated into monomers while the larger particles reduce in size. The size difference in the larger particles are reduced by etching and monomer concentration of the solution attains an equilibrium. When these particles are grown by increasing temperatures in the monomer saturated solution their growth are aided by the monomers which redeposit onto the particles enabling uniform growth. The plot shown in **Figure S4** also suggests this fact where the yield is replenished as the particles are grown. As no additional monomers are being injected into the solution this recovery of mass can only come from the monomers regorwing the particles. The monomers production and saturation by the etching step eliminates the competition of the larger particles with the smaller particles for growth as often observed in Ostwald ripening and in turn facilitates monodisperse growth.

Growing these particles in the stabilized 3:1 OLA: Cl solutions we see that even in the cases where the particle is stable in the solution and is not etched, they grow to form mono-disperse particles of size 7nm which is shown in the **Figure S5** which provides an apparent contradiction when compared to our story so far where we relied on the formation of monomers for size focusing. However, the observation can be explained by the fact that even though the seed does not etch it is protected or passivated from dynamic interactions with other particles by the OLA-CL complexes formed around it in the solution. This passivation of the seeds reduces the particle-particle interactions and thus we obtain monodisperse nanoparticles. Hence, in this report we have shown ways to control the dispersity of the nanoparticles by simply controlling the etching environment and suggests a way to reuse nanoparticles as seeds to produce new monodisperse nanoparticles.

1.5 Conclusion

In our investigation of the effects of OLA on $Cu_{2-x}S$ nanoparticles, we have conclusively shown for the first time that when present in excess, OLA etches the nanoparticles. The etching property scales with the relative OLA concentration and thus we can attain different levels of monomer saturation by tuning the amount of OLA present in the solution. We show that Chlorine could be used to stabilize the particles in solution as it complexes with the ligands which presents an alternative way to control the monomer concentration in the solution. The etching phenomenon when succeeded by growing of the particle by our heat-up method results in superior size focusing of nanoparticles with a size dispersity as low as 7%, as the monomers aid in the uniform growth of the particles, in contrast to those grown in solutions devoid of monomers which results in competitive particle growth associated with Ostwald ripening. In conclusion our post synthesis treatment suggests a way to transform a batch of nanoparticles of any size to any desired size while maintaining phase, crystallinity, morphology and provides significant advances to monodisperse growth control of nanoparticles. Furthermore, our novel approach to nanoparticle synthesis by means of reusing a batch of nanoparticles and to regrow them into a monodisperse set of nanoparticles of a specific size (8.5nm in our experiments) complements scalable high concentration nanomanufacturing providing a step further in the direction of large scale colloidal nanoparticle production and present the first ever concept of reusability in nanoparticles manufacturing.

1.6 Supplementary Information

XRD Data:

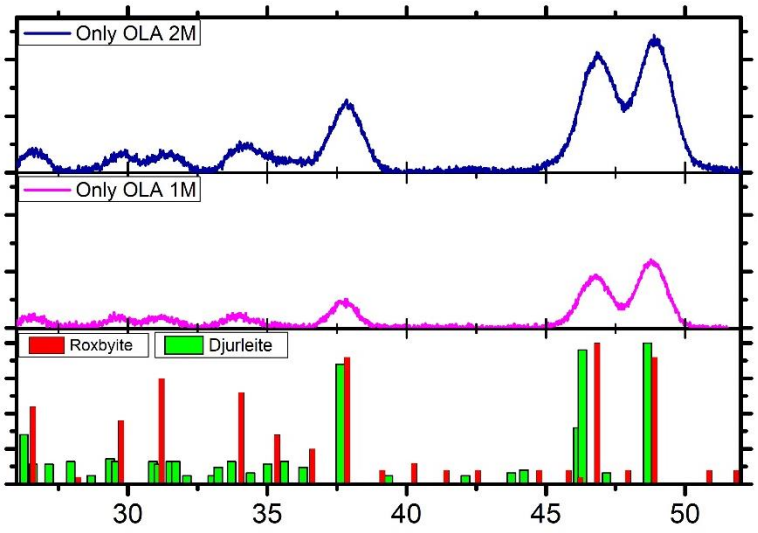

Figure S1: Shows the XRD plots of the particles after mixing with OLA solutions. The molarities indicated in the legend corresponds to the initial seed concentrations which were varied from 1M to 2M. This shows that the phase is consistently Roxbyite.

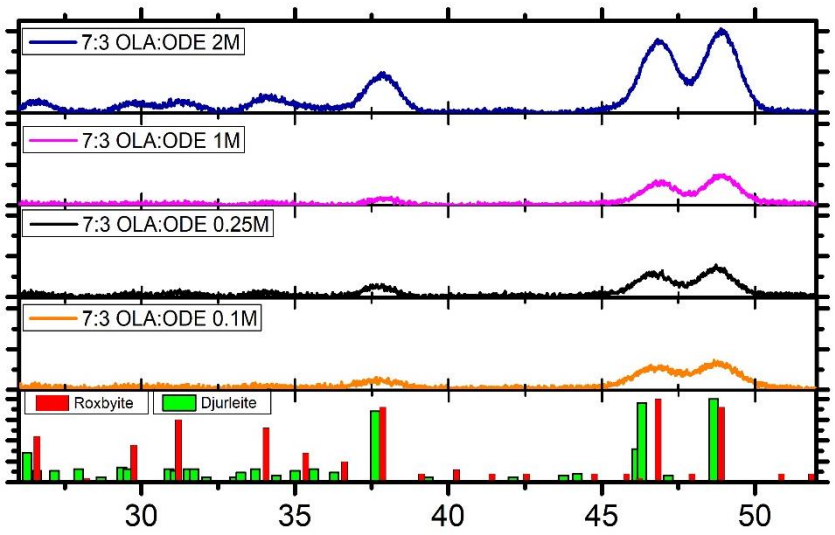

Figure S2: Shows the XRD plots of the particles after mixing with 7:3 OLA:ODE solutions. The molarities indicated in the legend corresponds to the initial seed concentrations which were varied from 0.1M to 0.25M to 1M to 2M. This shows that the phase is consistently Roxbyite.

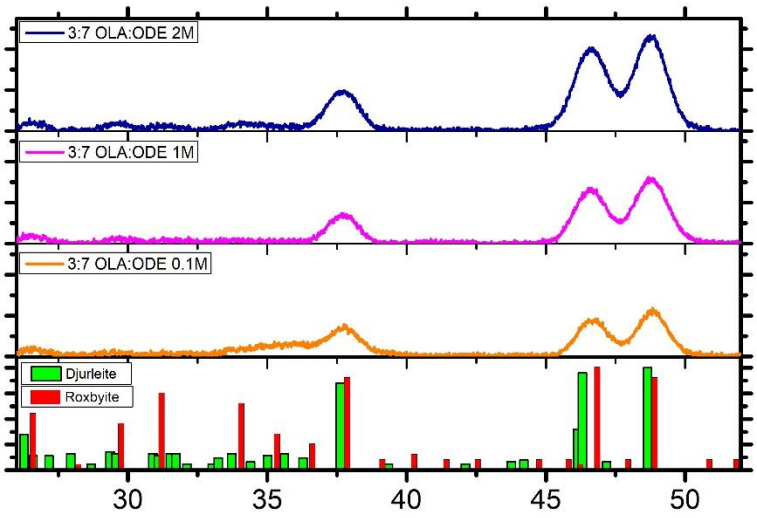

Figure S3: Shows the XRD plots of the particles after mixing with 3:7 OLA:ODE solutions. The molarities indicated in the legend corresponds to the initial seed concentrations which were varied from 0.1M to 1M to 2M. This shows that the phase is consistently Roxbyite.

These XRD plots confirm that in all our etching reactions the phase is maintained as Roxbyite.

Tables of yields for seeds in OLA:ODE solutions:

Table S1

Time (mins)	**OLA only (Yield %)**	**Cu monomer conc (Moles/L)**	**S Monomer Conc (Moles/L)**	**7:3 OLA:ODE (Yield %)**	**Cu monomer conc (Moles/L)**	**S Monomer Conc (Moles/L)**
10	40	0.58898	0.33156	59.8	0.39458	0.22221
30	30	0.68904	0.38804	60.9	0.38378	0.21613
60	20	0.78523		53.7	0.45445	0.25593
120	17	0.81468	0.4588	58.5	0.40734	0.2294

Time (mins)	3:7 OLA:ODE (Yield %)	Cu monomer conc (Moles/L)	S Monomer Conc (Moles/L)	ODE only (Yield %)	Cu monomer conc (Moles/L)	S Monomer Conc (Moles/L)
10	71	0.22772	0.12824	0.901	0.09811	
30	53	0.36906	0.20784			
60	47.566	0.41173	0.23187	0.87	0.11779	
120	48.89	0.40133	0.22602	0.88	0.1276	

Tables of yields for seeds in OLA:ODE solutions with Chlorine:

Table S2

OLA Vol%	Cl Vol %	Yield%
0	8	30
100	0	40
27.6	8	50
70	0	60
64.4	8	62
73.6	8	70
30	0	71
92	8	88
47.9	4.1	89
0	0	90
29.25	2.5	93
66.01	5.7	94

Regaining Yield after growth:

The following yield plot shows that when the seeds are regrown in the solution containing monomers the yield is replenished. As there was no external addition of monomers or material in the solution it suggests that the etched monomers are aiding the remaining particles to grow in size thus promoting uniform growth and reduce Ostwald ripening.

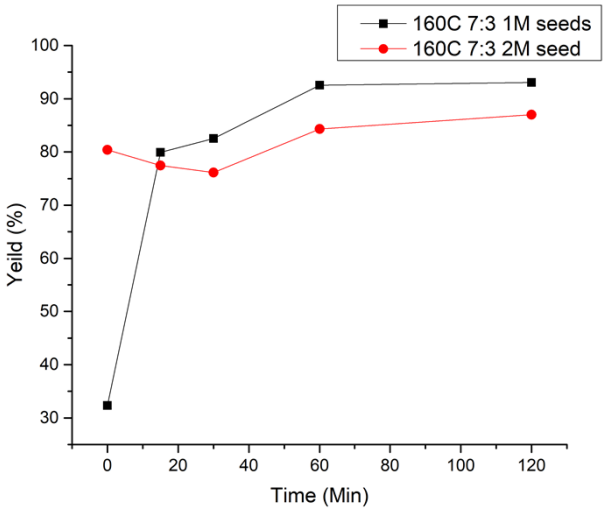

Figure S4. A yield plot representing the mass retained in solution at different time slices as the seeds are grown in the solution saturated with monomers. We see that the yield is replenished indicating that the monomers are re-growing on the remaining $Cu_{2-x}S$ particles resulting in monodisperse particle growth.

TEM of regrowth in the presence of Chlorine:

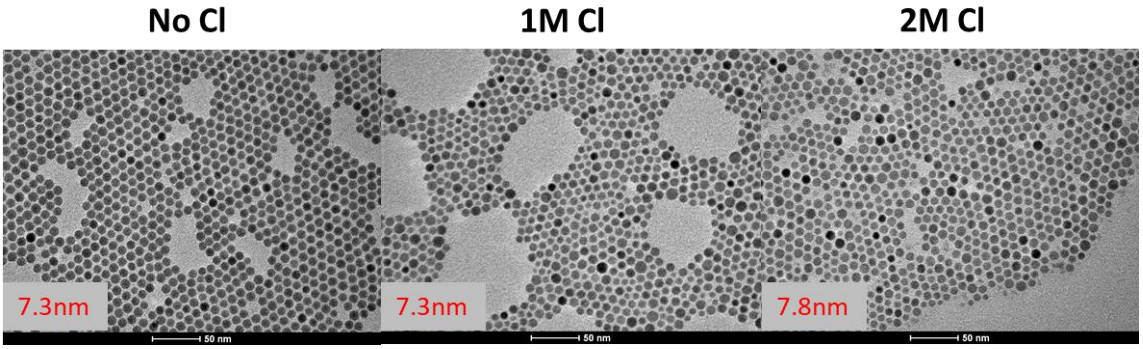

Figure S5. The final $Cu_{2-x}S$ nanoparticles obtained from re-growing seeds in a pure OLA solution with varying Chlorine concentrations. They all show the same particle size and dispersity indicating that in spite of the presence of Chlorine the particles grow monodisperse.

REFERENCES

[1] Claudia Coughlan; Maria Ibáñez; Oleksandr Dobrozhan; Ajay Singh; Andreu Cabot; Kevin M. Ryan. Chem. Rev. 117, 9, 5865-6109

[2] Jagiello, K., Chomicz, B., Avramopoulos, A. et al. Struct Chem (2017) 28: 635.

[3] Y. Volokitin: J. Sinzig; L. J. de Jongh; G. Schmid; M. N. Vargaftik; I. I. Moiseevi Nature volume384, pages621–623 (26 December 1996)

[4] Sagadevan Suresh, Semiconductor Nanomaterials, Methods and Applications: A Review, Nanoscience and Nanotechnology, Vol. 3 No. 3, 2013, pp. 62-74. doi: 10.5923/j.nn.20130303.06.

[5] Yue Wu, Cyrus Wadia, Wanli Ma, Bryce Sadtler, and A. Paul Alivisatos; Synthesis and Photovoltaic Application of Copper(I) Sulfide Nanocrystals; Nano Lett. 8, 8, 2551-2555

[6] Peter A. Ajibade and Nandipha L. Synthesis, Optical and Structural Properties of Copper Sulfide Nanocrystals from Single Molecule Precursors; Botha Nanomaterials 2017, 7, 32; doi:10.3390/nano7020032

[7] Josep Alberoa, John N. Clifforda, Emilio Palomares; Quantum dot based molecular solar cells; Coordination Chemistry Reviews 263–264 (2014) 53–64

[8] Sandra Dias, Kishan Lal Kumawat, Shinjini Biswas, S. B. Krupanidhi; Heat-up synthesis of Cu2SnS3 quantum dots for near infrared photodetection; RSC Adv., 2017, 7, 23301

[9] Sandra Dias, Kishan Lal Kumawat, Shinjini Biswas, S. B. Krupanidhi; Solvothermal Synthesis of Cu_2SnS_3 Quantum Dots and Their Application in Near-Infrared Photodetectors; Inorg. Chem. 56, 4, 2198-2203

[10] Sandra Dias and S B Krupanidhi; Cu2SnS3 nanostructures for inorganic–organic hybrid infrared photodetector applications; 2016 Mater. Res. Express 3 105006

[11] Sandra Dias, and S. B. Krupanidhi; Solution processed Cu2SnS3 thin films for visible and infrared photodetector applications; AIP Advances 6, 025217 (2016); doi: 10.1063/1.4942775

[12] Yong Lin Kong, Ian A. Tamargo, Hyoungsoo Kim, Blake N. Johnson, Maneesh K. Gupta, Tae-Wook Koh, Huai-An Chin, Daniel A. Steingart, Barry P. Rand,

and Michael C. McAlpine; 3D Printed Quantum Dot Light-Emitting Diodes Nano Lett. 14, 12, 7017-7023

[13] Sun L[1], Choi JJ, Stachnik D, Bartnik AC, Hyun BR, Malliaras GG, Hanrath T, Wise FW; Bright infrared quantum-dot light-emitting diodes through inter-dot spacing control; Nat Nanotechnol. 2012 May 6;7(6):369-73. doi: 10.1038/nnano.2012.63.

[14] Vanessa Wood and Vladimir Bulovic; Colloidal quantum dot light-emitting devices; Nano Reviews 2010, 1: 5202 - DOI: 10.3402/nano.v1i0.5202

[15] Zhenyu Yang, Oleksandr Voznyy, Mengxia Liu, Mingjian Yuan, Alexander H. Ip, Osman S. Ahmed, Larissa Levina, Sachin Kinge, Sjoerd Hoogland, and Edward H. Sargent; All-Quantum-Dot Infrared Light-Emitting Diodes; ACS Nano 9, 12, 12327-12333

[16] Gao, M.R.; Xu, Y.F.; Jiang, J.; Yu, S.H. Nanostructured metal chalcogenides: Synthesis, modification, and applications in energy conversion and storage devices. Chem. Soc. Rev. 2013, 42, 2986–3017.

[17] Goel S, Chen F, Cai W. Synthesis and Biomedical Applications of Copper Sulfide Nanoparticles: From Sensors to Theranostics. Small (Weinheim an der Bergstrasse, Germany). 2014;10(4):631-645. doi:10.1002/smll.201301174.

[18] Jongnam Park, Jin Joo, Soon Gu Kwon, Youngjin Jang, and Taeghwan Hyeon; Synthesis of Monodisperse Spherical Nanocrystals; Angew. Chem. Int. Ed. 2007, 46, 4630 – 4660

[19] Boles, M. A.; Engel, M.; Talapin, D. V. Self-Assembly of Colloidal Nanocrystals: From Intricate Structures to Functional Materials. Chem. Rev. 2016, 116, 11220−11289.

[20] Talapin, D. V.; Shevchenko, E. V.; Bodnarchuk, M. I.; Ye, X.; Chen, J.; Murray, C. B. Quasicrystalline Order in Self-Assembled Binary Nanoparticle Superlattices. Nature 2009, 461, 964−967.

[21] Ilka Kriegel, Chengyang Jiang, Jessica Rodríguez-Fernández, Richard D. Schaller, Dmitri V. Talapin, Enrico da Como and Jochen Feldmann; Tuning the Excitonic and Plasmonic Properties of Copper Chalcogenide Nanocrystals. J. Am. Chem. Soc. 2012, 134, 1583−1590.

[22] Joseph M. Luther1,2† , Prashant K. Jain1,2,3† , Trevor Ewers1,2 and A. Paul Alivisatos; Localized surface plasmon resonances arising from free carriers in doped quantum dots; Nat. Mater. 2011, 10, 361−366.

[23] Su-Wen Hsu, Kathy On, and Andrea R. Tao; Localized Surface Plasmon Resonances of Anisotropic Semiconductor Nanocrystals. J. Am. Chem. Soc. 2011, 133, 19072−19075.

[24] Wei Han, Luoxin Yi, Nan Zhao, Aiwei Tang, Mingyuan Gao and Zhiyong Tang; Synthesis and Shape-Tailoring of Copper Sulfide/Indium Sulfide-Based Nanocrystals J. Am. Chem. Soc., 2008, 130 (39), pp 13152–13161

[25] Luca De Trizio, Mirko Prato, Alessandro Genovese, Alberto Casu, Mauro Povia, Roberto Simonutti, Marcelo J. P. Alcocer, Cosimo D'Andrea, Francesco Tassone, and Liberato Manna; Strongly Fluorescent Quaternary Cu−In−Zn−S Nanocrystals Prepared from Cu1-xInS2 Nanocrystals by Partial Cation Exchange; Chem. Mater., 2012, 24 (12), pp 2400–2406

[26] Peng, X. G.; Wickham, J.; Alivisatos, A. P. Kinetics of II-VI and III-V Colloidal Semiconductor Nanocrystal Growth: "Focusing" of Size Distributions. J. Am. Chem. Soc. 1998, 120, 5343−5344.

[27] Clark, M. D.; Kumar, S. K.; Owen, J. S.; Chan, E. M. Focusing Nanocrystal Size Distributions via Production Control. Nano Lett. 2011, 11, 1976−1980.

[28] C.B. Williamson, D.R. Nevers, T. Hanrath, R.D. Robinson, "The Prodigious Effects of Concentration Intensification on Nanoparticle Synthesis: A High-Quality, Scalable Approach," J. Am. Chem. Soc. 137, 15843 (2015). DOI: 10.1021/jacs.5b10006

[29] Stefanos Mourdikoudis and Luis M. Liz-Marzán; Oleylamine in Nanoparticle Synthesis Chem. Mater., 2013, 25 (9), pp 1465–1476

[30] Mark Green; The nature of quantum dot capping ligands; J. Mater. Chem., 2010, 20, 5797–5809

[31] G. Krishnamurthy Grandhi, Arunkumar M., and Ranjani Viswanatha; Understanding the Role of Surface Capping Ligands in Passivating the Quantum Dots Using Copper Dopants as Internal Sensor; J. Phys. Chem. C 2016, 120, 19785−19795

[32] Natalia Razgoniaeva, Mingrui Yang, Paul Garrett, Natalia Kholmicheva, Pavel Moroz, Holly Eckard, Luis Royo Romero, Dmitry Porotnikov, Dmitriy Khon, and Mikhail Zamkov; Just Add Ligands: Self-Sustained Size Focusing of Colloidal Semiconductor Nanocrystals; Chem. Mater. 2018, 30, 1391−1398

[33] Semiconductor Nanocrystals and Silicate Nanoparticles, Volume 118, (Pg 92) Xiaogang Peng, D. M. P. Mingos Springer Science & Business Media, Nov 3, 2005 - Science

CHAPTER 2

HIGH CONCENTRATION PURE PHASE COPPER-TIN-SULPHIDE NANOPARTICLES SYNTHESIS

Shinjini Biswas, Johnathan Neff, Zhiqi Wang, and Richard Robinson

– Work in progress

Abstract

Achieving phase purity in Copper Tin Sulphide (CTS) nanoparticles has been a challenge due to the distinct similarities of Mohite (Cu_2SnS_3) and Kuramite phase (Cu_3SnS_4). In this work we present a synthesis method for the production of pure tetragonal Mohite phase of CTS. Our work builds on the previous developments made by the group in scalable nanomaterials manufacturing via high concentration synthesis. We extend the study by using a second metal precursor and show the synthesis of a ternary semiconductor that finds important application as an absorber in tin film photovoltaics. We show that using our heat up method we can segregate the two CTS phases and produce pure Mohite phase at 150°C and pure Kuramite phase at 185°C. Further we probe the effect of changing the copper to tin ratios while maintaining Mohite phase purity and report a distinct improvement in the particle size deviation. The improvement is much more spectacular when a small change in the Cu(I) : Sn(IV) ratio from 1:1 to 1:2 shows a decrease in standard deviation in particle size from 6.5nm to 0.5nm. The influence of the Tin valency and ratio on the final size of the particles show a decrease in particle

size with increasing Tin concentration which is consistent with similar studies in copper selenides.

2.1 Introduction

The world's energy demands of today is on a steady rise especially for the growing countries[1] (**Figure 2.1**) and the non-renewable energy sources which still form the backbone for the world's sustenance is rapidly depleting. To focus on rapid development of renewable resources is now a matter of urgent importance if we are to sustain and progress our modern lifestyles worldwide.

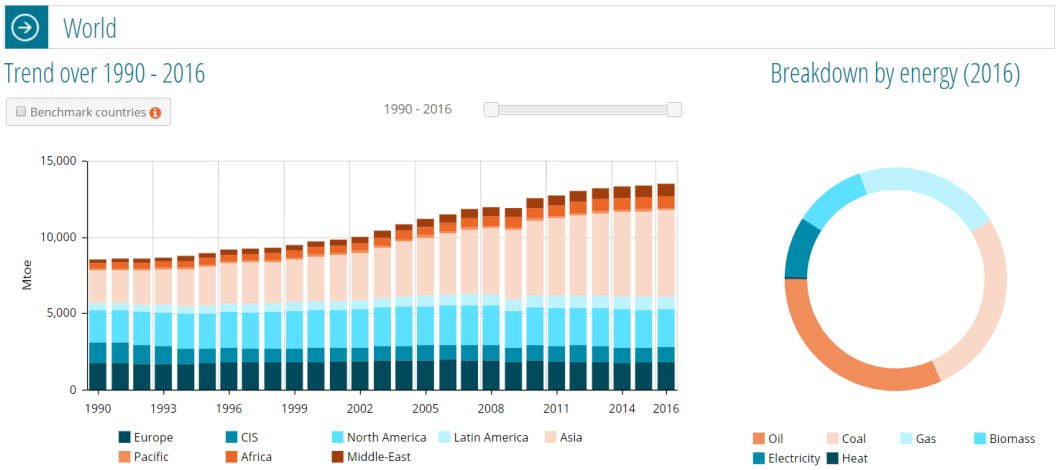

Figure 2.1. World's Energy Consumption Statistics from 1990 to 2016 as reported in the Global Energy Statistical Yearbook 2017 [1].

Solar energy is one emerging renewable energy source alternative that has inspired a lot of research efforts in the past few years [2]. However, owing to its relatively low efficiency and

reliability when compared to coal or oil it has not been able to replace the latter as a dominant source of sustainable energy.[3] Photovoltaics rely on the maximum utilization of the solar spectrum aiming to absorb light from a majority of the wavelengths to provide the optimum electrical output. One of the challenges in obtaining a high efficiency is the discrepancy between the incident spectrum and the energies actually absorbed. The semiconductors absorb energies corresponding to their bandgap and above, to produce electron-hole pairs and in turn produce electricity. The remaining energies are lost and so we see a drastic reduction in efficiency. To combat this issue efforts have been made in synthesizing advanced materials with increasingly higher absorption coefficients [4]. Nanoparticles in particular owing to their size dependent properties is emerging as a prominent contender in the development of the next generation solar cells [5].

Chalcogenides especially copper-based ternary and quaternary systems are an emerging p-type semiconductor nanomaterial that is widely preferred as an absorber in photovoltaic devices. Other opto-electronic materials like cadmium or lead chalcogenides have reported efficiencies of up to 16.8% [6] however due to their toxicity their use in most devices have been restricted or even banned. Copper-metal- chalcogenides provide a non-toxic relief in this respect where certain nanocrystals of Cu (In, Ga) (S, Se) have achieved efficiencies of around 10% [7] however the abundancy of Indium and Gallium is an imminent drawback in its commercial production. Copper Tin Sulphide (CTS) with its varying stoichiometries are recently proving to be a promising material in this respect with absorption coefficients of 10^4-10^5 cm^{-1} with an optimal band gap between (1.1-1.4eV) [8]. The abundancy of tin surpasses most other metals used for ternary copper chalcogenides thus providing a cheaper alternative.

The Cu2SnS3 phase termed as Mohite phase has widely known applications both in photovoltaics as well as in the development of IR photodetectors.[9-11] Mohite Quantum Dots are emerging as viable materials for hybrid Inorganic and Organic devices as well [12]. However. this phase is very similar to Kuramite phase of CTS i.e. Cu3SnS4 which often cause problems in obtaining phase purity when synthesizing Mohite CTS. Our report shows a method of separating these two phases and obtaining pure Mohite CTS phase.

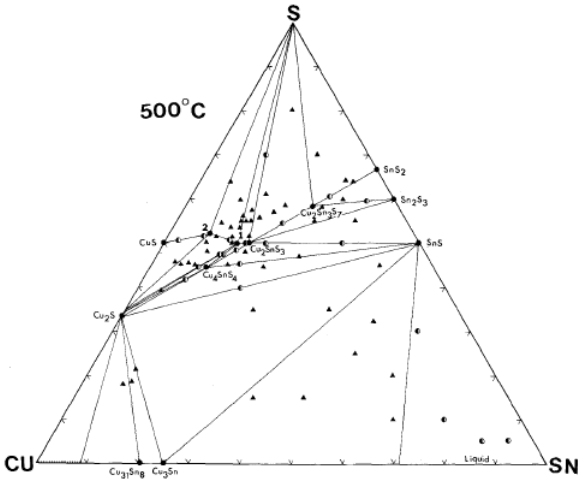

Figure 2.2. The phase diagram of materials of varying stoichiometries containing Copper, Tin and Sulphur. The ternary compounds are shown in the center of the diagram and efforts are made to synthesize these phases in purity.[13]

To establish Copper chalcogenides especially CTS as a commercially viable material for large scale incorporation in solar cells its synthesis process flow needs to be optimized. The main challenges for manufacturing of CTS nanoparticles is maintaining phase purity and developing a process flow that is easily scalable. The phases possible for CTS are shown in **Figure 2.2[13]** and synthesis procedure currently struggle in attaining one phase with consistent crystal

structure [13]. Currently the synthesis practices in place for obtaining high quality nanoparticles include the hot-injection method however successful implementation of this technique involves optimization of a wide range of parameters [14][15] especially for the synthesis of ternary compounds where there is more than one metal precursor. The other drawback to this method is that it is not readily scalable hence high purity nano-particles are formed from small-scale reactions proving to be a significant challenge for nanoparticle commercialization.

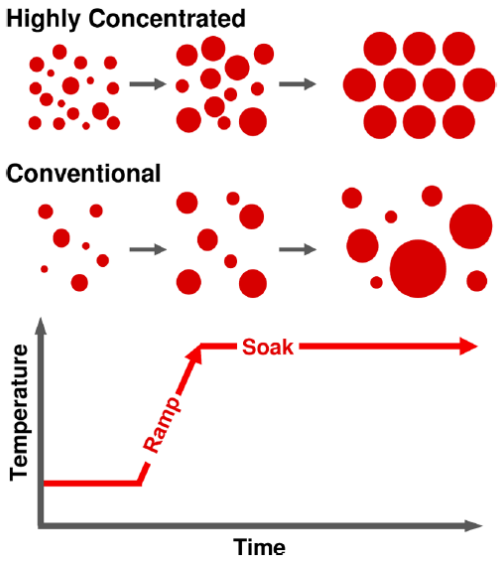

Figure 2.3. High Concentration nanoparticle synthesis procedure using a ramp and soak heat-up method highlighting the superior quality of particles produced as compared to conventional dilute synthesis. [16]

Our group developed a high concentration synthesis procedure which utilized a heat-up method where particles are mixed often in a one-pot synthesis and are ramped up to a high temperature where it is soaked for an amount of time as shown in **Figure 2.3**. This ramp and soak technique

is designed to operate in regimes of high concentrations which enables decoupling of the precursor mixing dynamics and the growth mechanism [16]. This method is seen to reduce the sensitivity to external parameters making it suitable for scalable nanomanufacturing. Our report here is an extension of this study reporting the synthesis of phase pure CTS using the afore mentioned high concentration approach, hence providing a scalable method of CTS nanoparticle production. Our results show a convenient control over the CTS phase and production of particles exhibiting bandgaps matching those required for most photovoltaic applications.

2.2 Materials

The following chemicals were used as received: Oleylamine (OLA, 98% primary amines), 1-octadecene (ODE, 90%), Copper(I) chloride (99.995%), Copper (II) chloride (99%), Tin (II) Chloride (98%), Tin (IV) Chloride (99.995%) and elemental sulfur (purified by sublimation, particle size~100 mesh) were purchased from Sigma-Aldrich. Hexanes (BDH ACS Grade) and ethanol (Ethanol, 200 proof, Anhydrous KOPTEC USP) were purchased from VMR International.

2.3 Experimental Procedures

Cu(I)+Sn(II) solution Preparation –

1:1 ratio:

500mM (0.495 g) of CuCl and 500mM (0.948 g) of $SnCl_2$ is mixed with 7 ml of Oleylamine (OLA) and 3ml of 1-Octadectene (ODE) in a round bottom flask. The mixture is heated to 50°C,

degassed and heated up to 110 °C under vacuum, where it is allowed to mix for 2 hours until the solution becomes clear and homogeneous indicating that the salts are dissolved. The solution is then cooled down to 50 °C and put under nitrogen.

1:2 ratio:

334mM of CuCl and 666mM of $SnCl_2$ is mixed and treated in an identical manner as dictated above.

Cu(I)+Sn(IV) solution Preparation –

500mM of CuCl and 500mM of $SnCl_4$ is mixed with 7 ml of Oleylamine (OLA) and 3ml of 1-Octadectene (ODE) in a round bottom flask and treated in the exact manner as stated above. The corresponding molar ratios were calculated for 1:2 Cu(I): Sn(IV) synthesis and treated likewise.

Cu(II)+Sn(II) solution Preparation –

500mM of $CuCl_2$ and 500mM of $SnCl_2$ is mixed with 7 ml of Oleylamine (OLA) and 3ml of 1-Octadectene (ODE) in a round bottom flask and treated in the exact manner as stated above. The corresponding molar ratios were calculated for 1:2 Cu(II): Sn(II) synthesis and treated likewise.

Cu(II)+Sn(IV) solution Preparation –

500mM of $CuCl_2$ and 500mM (0.948 g) of $SnCl_4$ is mixed with 7 ml of Oleylamine (OLA) and 3ml of 1-Octadectene (ODE) in a round bottom flask and treated in the exact manner as stated

above. The corresponding molar ratios were calculated for 1:2 Cu(II): Sn(IV) synthesis and treated likewise.

Sulphur Solution Preparation –

In a separate round bottom flask 1.6 g of Sulfur is mixed with 7 ml of OLA and 3 ml of ODE. The mixture is degassed and put under nitrogen before heating it up to 110 °C where it is allowed to mix for 1 hour. The solution is then cooled down to 50 °C.

Copper Tin Sulphide Synthesis and Growth Procedure – (Figure 2.4)

1 ml of the sulfur solution is taken and added to the Copper + Tin solution (using the required valency and ratio) at 50 °C. The solution is stirred for 10 mins and heated to 150°C with a ramp-rate of 5°/min. Aliquots were taken at intervals (75°C, 100°C, 150°C). After reaching 150°C the solution is soaked at the temperature for 2hrs with aliquots being taken at 10min, 30mins, and 1hr after start of soak. The solution is then brought to room temperature. The aliquots and the final solution is poured out into centrifuge tubes with excess of ethanol. The product is then centrifuged for 5 min at 4400 rotations per minute. Then the solution is washed 3 times by resuspending in hexane, precipitating by ethanol and centrifuging as done earlier.

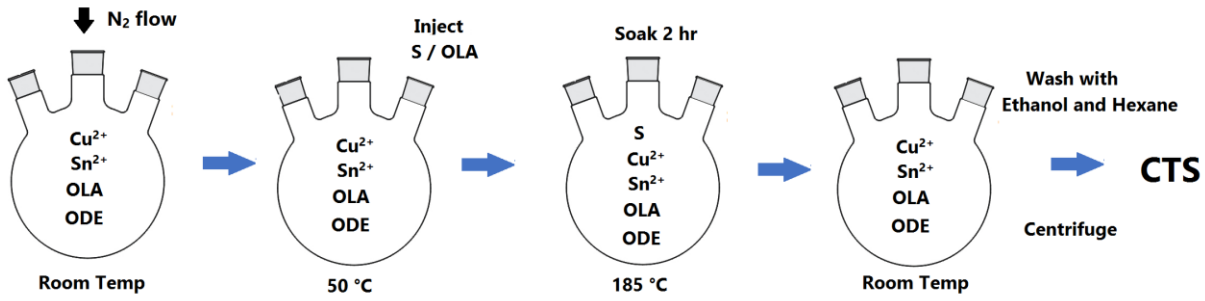

Figure 2.4. Schematic representation of the Copper Tin Sulphide synthesis procedure.

Characterization methods –

X-ray powder diffraction (XRD) data were collected on a Bruker D8 General Area Detector Diffraction System (Cu Kα radiation, ~ 1.54 Å). Samples were washed with ethanol, centrifuged, and resuspend in hexane three times. After the three wash, the samples were dried overnight before XRD analysis.

Raman Spectroscopy analysis was performed on the Reinshaw InVia Raman microscope at CCMR facility at Cornell. Samples were washed with ethanol, centrifuged, and resuspend in hexane three times. After the three wash, the samples were dried overnight. Samples for the Raman analysis were prepared by placing a small amount of cleaned dried nanoparticles onto the stage.

Ultra Violet – Visible Spectroscopy (UV-Vis) analysis was performed on a Variam Carry 5000. Samples for UV – Vis analysis were prepared by adding a few micrograms of the cleaned nanoparticle powder into toluene solution in a UV-Vis spectrometer vial before inserting it into the spectrometer. The required calibration was done by subtracting background data of the toluene itself before acquiring the absorption data of the particles.

2.4 Results and Discussions

To achieve phase pure Copper Tin Sulphide we extended the high concentration synthesis method developed by our group to include two metal cations instead of only copper. As in most research on nanoparticle synthesis tuning the parameters, both of the physical environment and that of the materials are crucial to maintain phase purity, size, and yield.

Kuramite – Mohite Phase dependence on Temperature:

Temperature is widely seen as one of the most important physical parameters that controls the synthesis of nanoparticles [17][18]. To understand the effect of temperature on our synthesis of pure phase Copper-Tin-Sulphide we investigate the crystal structure of the particles made from Cu(I) and Sn(II) in a ratio of 1:1 after heating and soaking at 185°C and 150°C. On analyzing the particles with the help of XRD we obtained signatures of Kuramite (Cu_3SnS_4) and Mohite (Cu_2SnS_3) phases of Copper-Tin-Sulphide. The results are shown in **Figure 2.5** where **a)** shows the XRD peak evolutions of particles heated to and soaked at 185°C. **Figure 2.5 b)** shows the XRD peak evolution of particles that were heated to and soaked at 150°C.

Kuramite and Mohite are notorious in showing very similar XRD peak signatures with very slight differences shown in the formation of minor peaks at 36 and 45 in the case of Kuramite. In addition to this the peak at 47 is much more pronounced and intense in the case of Kuramite as compared to Mohite. Following these references our data suggests that the particles soaked at a higher temperature of 185°C (**Figure 2.5a**) show Kuramite phase as the peak at 47 is relatively more intense, whereas those soaked at a lower temperature of 150°C (**Figure 2.5b**) show Mohite phase. The minor peaks are hard to distinguish from the noise as the particles themselves are nano-sized. We also observe that as the particles are heated up during the ramp the peaks become more distinct indicating that the particles become increasingly crystalline. On soaking the particles from 30 mins to 1 hr. we see the peaks narrowing indicating that the particles are growing in size.

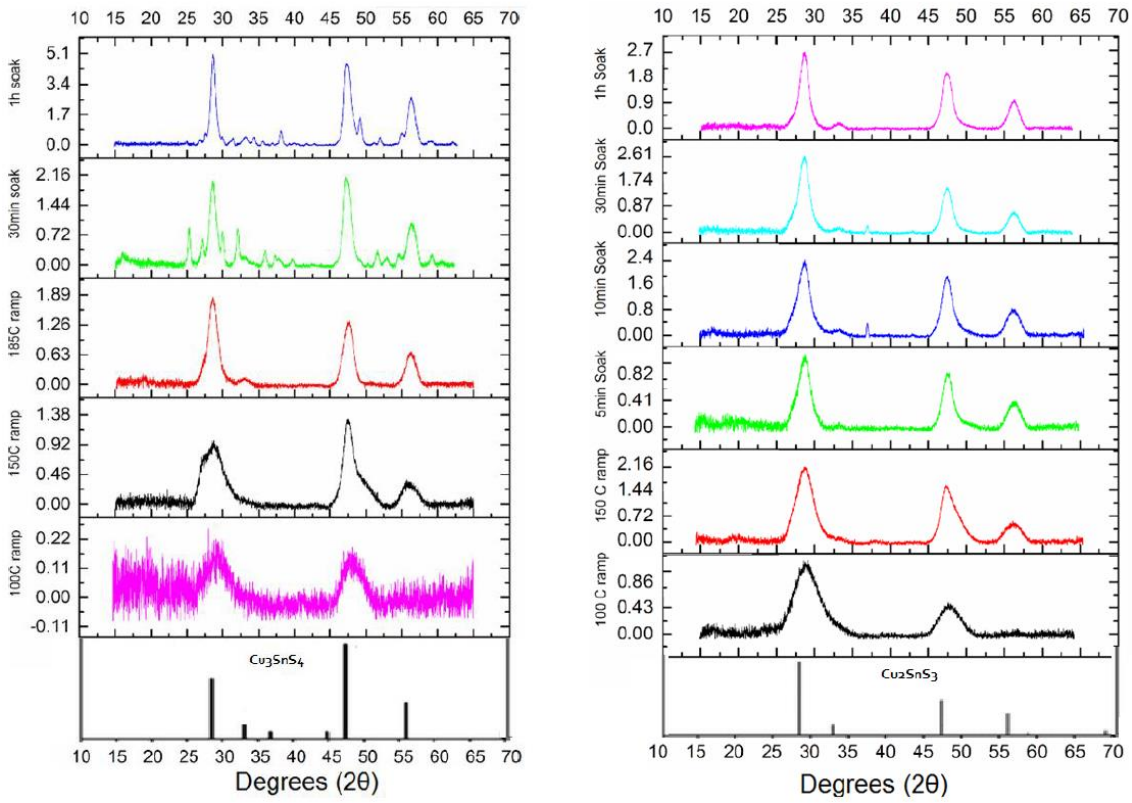

Figure 2.5. *XRD peaks at different time stamps across ramp temperatures and soak times of CTS nanoparticles synthesized from 1:1 ratio of Cu(I): Sn(II) metal precursors heated to a)185 C (aliquots at 100C, 150C, 185C, 30 mins soak and 1hr soak) showing Kuramite (Cu_3SnS_4) formation; b) 150 C (aliquots at 100C, 150 C, 5 mins soak, 10 mins soak, 30 mins soak and 1hr soak) showing Mohite (Cu_2SnS_3) formation.*

As the XRD peaks for Kuramite and Mohite are very similar there may be questions regarding the purity of the phase obtained by either procedure. **Figure 2.6** shows the Raman Spectra of the nanoparticles soaked at 150°C (left) and those soaked at 185°C (right). The 317-peak shown in **Figure 2.6 left** is indicative of the orthorhombic Kuramite [19] and the absence of other peaks relative to this is indicative that this phase occurs without any other binary impurity. In **Figure 2.6 right** we observe the formation of 3 peaks at – 297, 321 and 352. This is indicative of the tetragonal phase of Cu2SnS3 or Mohite [20].

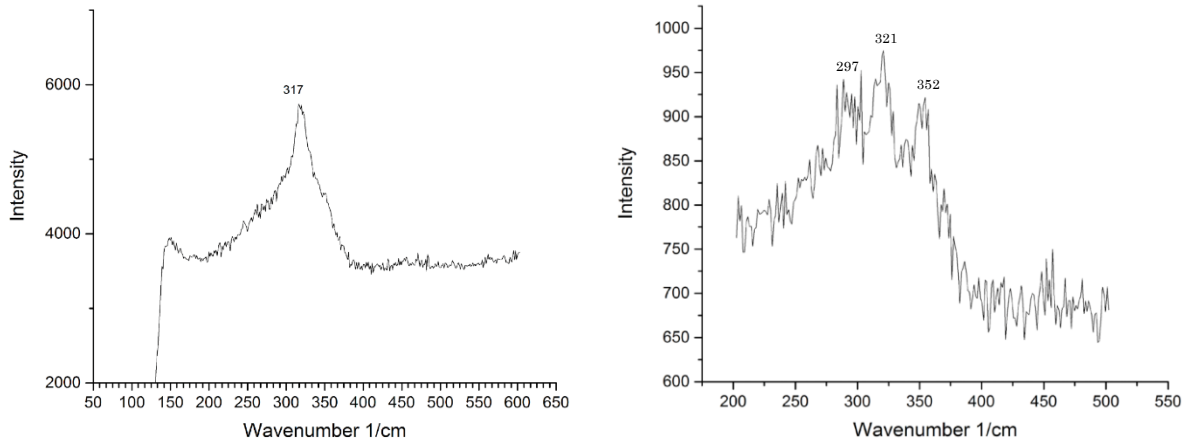

Figure 2.6. *Raman Spectra of CTS nanoparticles synthesized form 1:1 Cu(I): Sn(II) metal precursor ratio heated to and soaked at: (left)185 C showing distinctive peak at 317, indicative of orthorhombic Kuramite; (right) 150C showing 3 peaks at 297, 321 and 352, indicative of tetragonal Mohite.*

It is widely shown in literature that temperature is key for growth of a nanoparticle. To investigate the extent of temperature dependence of the particle size we calculate the nanoparticle sizes with the help of Debye Scherrer analysis. The following table summarizes the particle sizes at each time slice for both procedures.

Ramp/Soak	Size (nm)
100C ramp	2
150C ramp	3-4
5min soak	4-5
10min soak	4-5
30min soak	5-8
1h soak	7-10

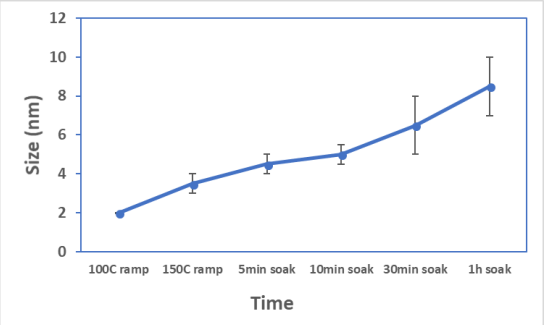

Figure 2.7. *CTS Nanoparticles synthesized from 1:1 Cu(I): Sn(II) precursor ratios heated to 150 C (left) Table with the particle size for each time slice (right) Plot of the particle sizes with error.*

Ramp/Soak	Size (nm)
150C ramp	3-7
185C ramp	5-6
30min soak	8-10
1h soak	8-13

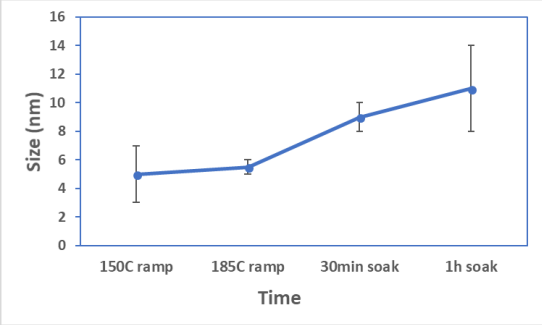

Figure 2.8. *CTS Nanoparticles synthesized from 1:1 Cu(I): Sn(II) precursor ratios heated to 185°C (left) Table with the particle size for each time slice (right) Plot of the particle sizes with error.*

Comparing **Figure 2.7** and **2.8** we see that when the particles are soaked at a higher temperature of 185°C they grow to a larger final average particle size of 10.5nm whereas those that are soaked and grown at 150°C attain a final average particle size of 8.5 nm. We deduce that particle size increases not only with ramp but the ultimate temperature the particles are soaked at.

CTS Nanoparticles Dependence on Cu to Sn Ratio:

a) Cu (I) : Sn (II) Ratios:

To understand the effects of varying the Copper to Tin ratio on the CTS nanoparticle synthesis and growth we repeat the high concentration synthesis with 1:2 molar ratios of the metal precursors in the initial solution which is heated and soaked at 150°C. **Figure 2.9** shows the Raman of the CTS nanoparticles synthesized from 1: 2 Cu(I): Sn(II) ratio which suggests that the particles regardless of the ratio consistently forms pure Mohite (Cu_2SnS_3) phase. It shows the similar 3 peaks that were seen previously indicating the particles are tetragonal in nature. The relative absence of other peaks suggest that the particles do not show binary phases or other impurities.

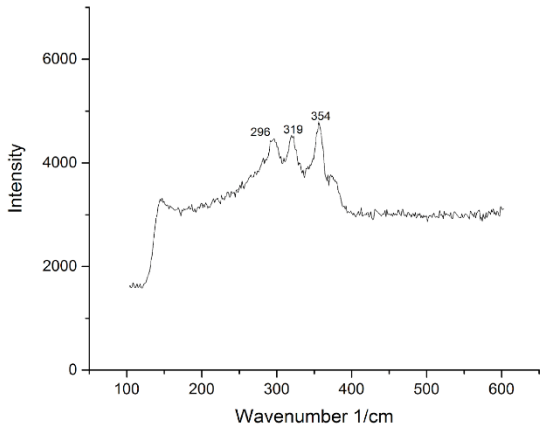

Figure 2.9. *Raman Spectra of CTS Nanoparticles synthesized from 1:2 Cu(I): Sn(II) precursor ratios heated to 150°C showing 3 distinct peaks indicative of tetragonal Mohite CTS.*

Ramp/Soak	Size (nm)
100C ramp	3
150C ramp	5
5min soak	6-7
10min soak	6-7
30min soak	7
1h soak	7-8
2h soak	10-12

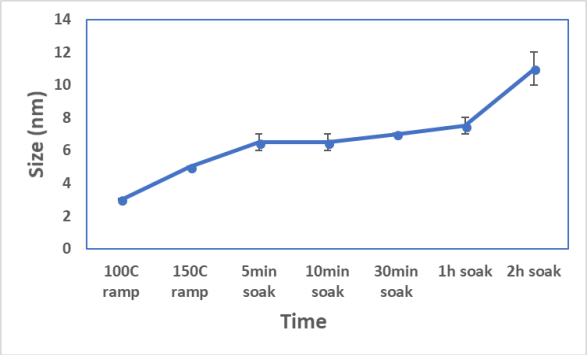

Figure 2.10. *CTS Nanoparticles synthesized from 1:2 Cu(I): Sn(II) precursor ratios heated to 150°C (left) Table with the particle size for each time slice (right) Plot of the particle sizes with error showing maximum average particle size as 8nm after 1hr.*

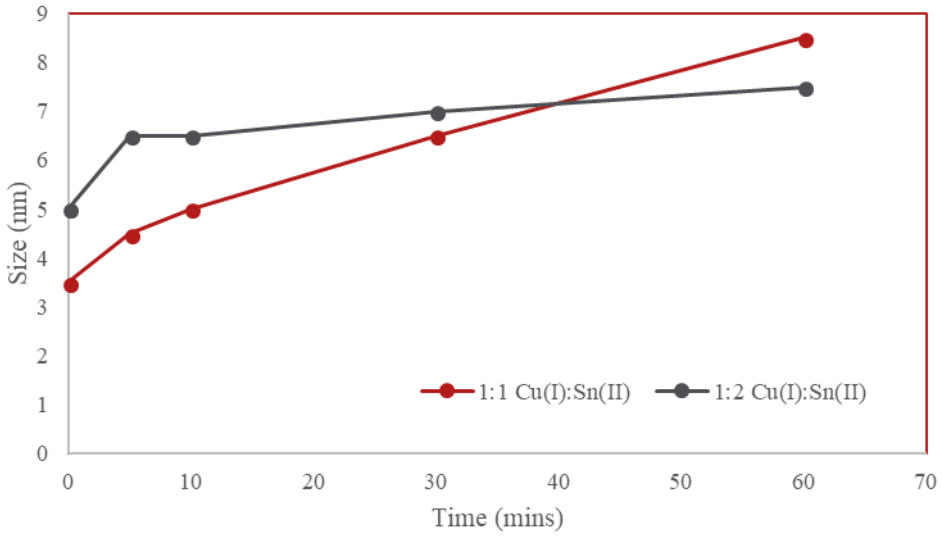

Figure 2.11. *Size Comparison of CTS nanoparticles while growing in reactions with 1:1 Cu(I):Sn(II) (red) and 1:2 Cu(I):Sn(II)(Black). Shows that with increasing Sn(II) ratio the particle size plateaus to a smaller NP size (7.5nm)*

Analysis of the corresponding particle sizes lead us to observe in **Figure 2.10** that the maximum average particle size now is 8nm. When comparing this with **Figure 2.7** where 1:1 Cu(I): Sn(II) ratio was heated to 150°C we see that a lower Sn(II) content corresponded to a ever slightly

higher final average particle size of 8.5nm whereas on doubling the molar concentration of Sn(II) to that of Cu(I) we see an decrease in the final particle size to 7.5nm while maintaining the same temperature of 150°C. Figure 2.11 illustrates this difference as shows the clear plateauing of the final NP size as the Sn(II) ratio is doubled. This enables us to consistently produce phase pure Mohite phase of CTS but vary the particle sizes. However, as this size difference falls within the error of the Debye Scherrer analysis we need further characterization methods like TEM to produce a more conclusive result.

b) Cu (II) : Sn (II) Ratios:

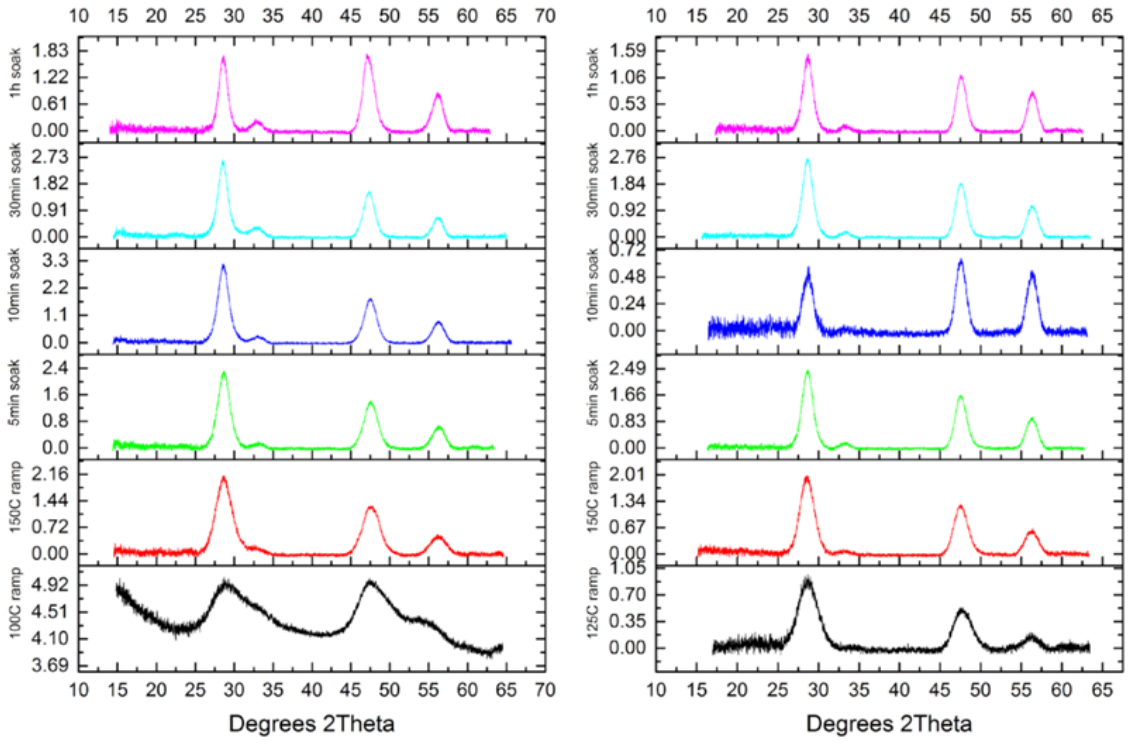

Figure 2.12. *XRD peaks at different time stamps across ramp temperatures and soak times of CTS nanoparticles heated to 150°C synthesized from: (left) 1:1 ratio of Cu(II):Sn(II) metal precursors (aliquots at 100°C, 150°C, 5 mins soak, 10mins soak, 30 mins soak and 1hr soak); (right) 1:1 ratio of*

Cu(II):Sn(II) metal precursors (aliquots at 125°C, 150°C, 5 mins soak, 10 mins soak, 30 mins soak and 1hr soak). Both show Mohite (Cu_2SnS_3) formation.

Figure 2.12 shows the XRD of CTS nanoparticles synthesized from precursors with Cu(II) and Sn(II) excitation states in ratios 1:1 and 1:2 heated to and soaked at 150°C. We see from the figure that particles prepared by both ratios yeild the same Mohite phase of CTS.

Figure 2.13 shows the size analysis of the particles formed from 1:1 and 1:2 ratios of Cu(II) to Sn(II) when heated to 150°C. Similar to our previous observation, we do not see a drastic difference in final particle size after soak when Cu(II) is reacted instead of Cu(I) with Sn(II) for both ratios. As shown the 1:1 Cu(II): Sn(II) reaction shows a maximum final particle size of 7nm while 1:2 Cu(II): Sn(II) reaction shows 6nm. We can see again that a higher Sn(II) ratio again plateaus the particle size to a lower final size as shown in figure 2.14.

Ramp/Soak	Size (nm)
150C ramp	3
5min soak	4
10min soak	5
30min soak	5-6
1h soak	5-7

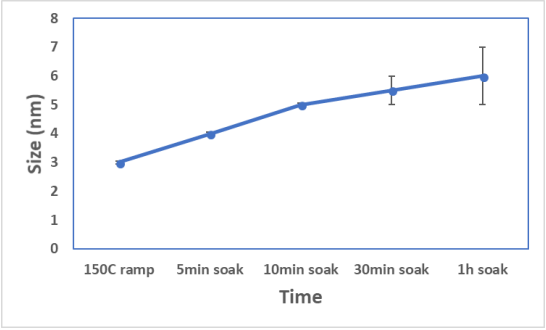

Ramp/Soak	Size (nm)
150C ramp	4
5min soak	5
30min soak	5-6
1h soak	6
2h soak	6-7

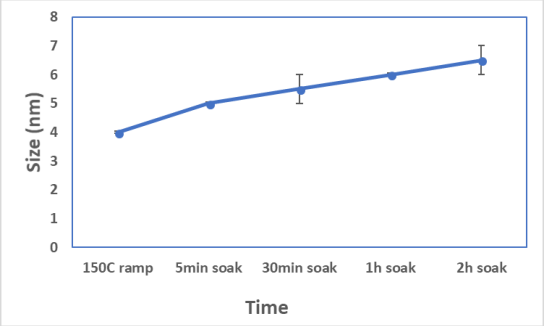

Figure 2.13. *CTS Nanoparticles synthesized by heating to 150°C: (Top row) 1:1 Cu(II): Sn(II) precursors (left) Table with the particle size for each time slice (right) Plot of the particle sizes with error showing maximum average particle size as 6nm. (Bottom row) 1:2 Cu(II): Sn(II) precursors (left) Table with the particle size for each time slice (right) Plot of the particle sizes with error showing maximum average particle size as 6.5nm.*

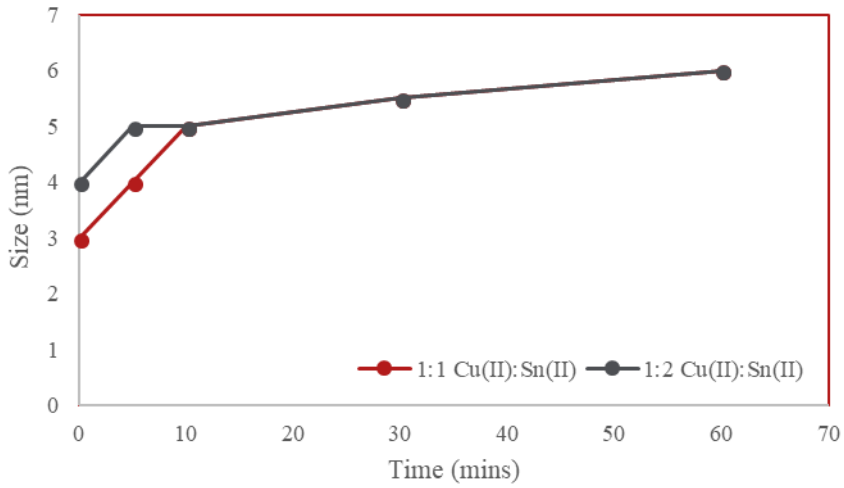

Figure 2.14. *Size Comparison of CTS nanoparticles while growing in reactions with 1:1 Cu(II):Sn(II) (red) and 1:2 Cu(II):Sn(II)(Black). Shows that with increasing Sn(II) ratio the particle size plateaus to a smaller NP size (6.5nm)*

c) Cu(I) : Sn (IV) Ratios:

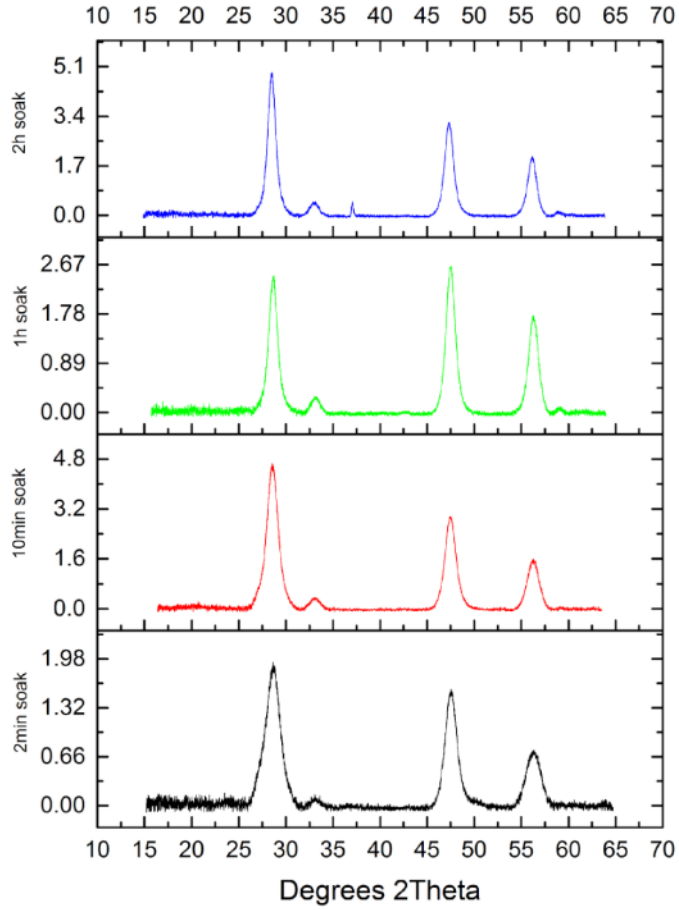

Figure 2.15. *XRD peaks at different time stamps across ramp temperatures and soak times of CTS nanoparticles heated to 150°C synthesized from 1:2 ratio of Cu(I): Sn(IV) metal precursors (aliquots at 2 mins soak, 10 mins soak, 1 hr soak and 2hr soak) showing very crystalline Mohite (Cu_2SnS_3) formation.*

Figure 2.15 shows the XRD of 1:2 Cu(I): Sn(IV) reaction when heated to 150 C where we see very clear distinct narrow peaks suggesting the particles are pure Mohite and relatively larger that our previous experiments. On comparing the time slices from the XRD data seen from previous reactions we see that even at 2 mins soak the particles are completely formed and crystalline in nature and already exhibits a narrow peak. This suggests that the reactivity of

Cu(I) with Sn(IV) is the fastest among all copper tin combinations resulting in faster reaction, nucleation, and growth.

Figure 2.16 shows the size analysis of the particles obtained after the reaction of 1:1 and 1:2 ratios of Cu(I) to Sn(IV). The difference seen in the final average particle size after soak is much more drastic as compared to any of the previous reactions. The 1:1 Cu(I): Sn(IV) reaction shows a final particle size of 27nm while 1:2 Cu(I): Sn(IV) reaction shows an average final particle size of only 8nm. The comparative sizes obtained on growing these particles as shown in **figure 2.17** show that a high Sn(IV) concentration shows a distinct plateauing of the NP size to 8nm while the reaction with lower Sn(IV) concentration shows almost an exponential increase in the growth size. This seems to suggest that the reactivity of Sn(IV) has a role in the nucleation and growth rates of CTS NPs.

Ramp/Soak	Size (nm)
150C ramp	4 (single peak)
185C ramp	7
30min soak	9-14
1h soak	22-35nm

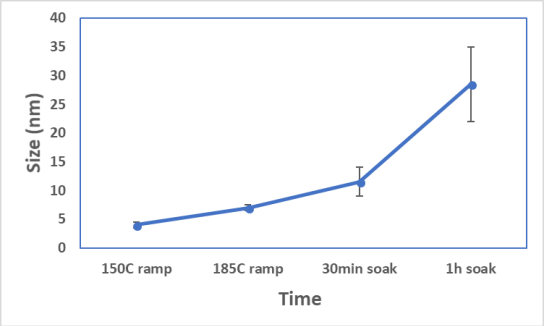

Ramp/Soak	Size (nm)
2min soak	4-6
10min soak	6-7
1h soak	8
2h soak	9

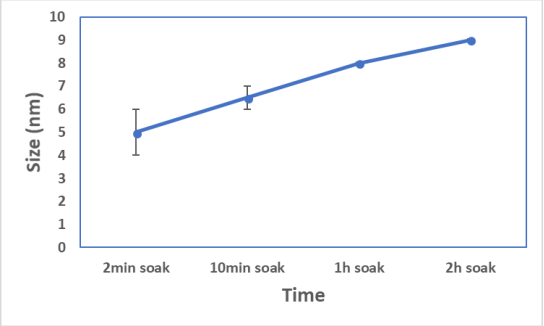

Figure 2.16. *CTS Nanoparticles synthesized by heating to 150°C: (Top row) 1:1 Cu(I): Sn(IV) precursors (left) Table with the particle size for each time slice (right) Plot of the particle sizes with error showing maximum average particle size as 27nm. (Bottom row) 1:2 Cu(I): Sn(IV) precursors (left) Table with the particle size for each time slice (right) Plot of the particle sizes with error showing maximum average particle size as 9nm.*

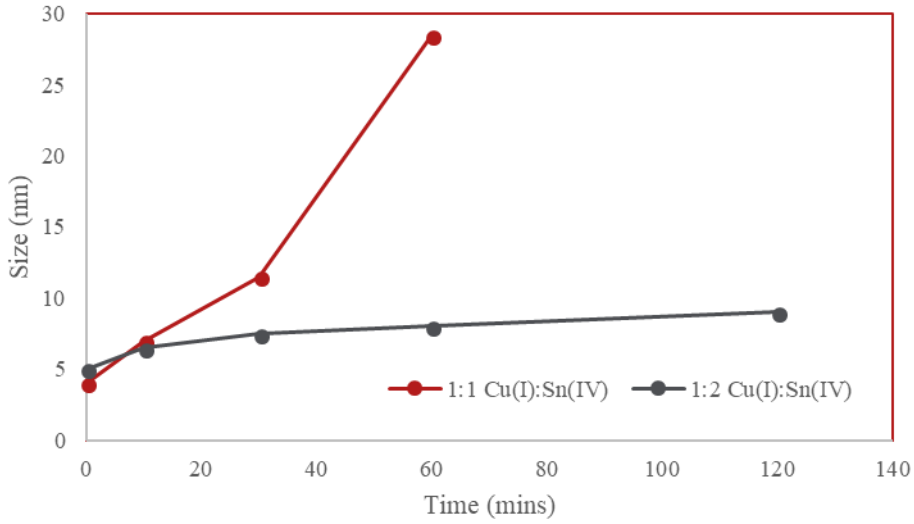

Figure 2.17. *Size Comparison of CTS nanoparticles while growing in reactions with 1:1 Cu(I):Sn(IV) (red) and 1:2 Cu(I):Sn(IV)(Black). Shows that with increasing Sn(II) ratio the particle size plateaus to a smaller NP size (8nm).*

From our data and analysis, observe that with increasing Tin concentration there is a consistent decrease in particle size when Tin is present in excess, regardless of the Copper valency. Xian Liang Wang, et al, findings on Copper Tin Selenide nanocrystals reports that with increasing Tin molar concentration there is an observable decrease in the particle size. Extrapolating this to our data we can see a match with our last combination. When all our pieces of data are viewed together they suggest that the reactivity of Copper to Tin plays a vital role in guiding the rates

of nucleation and growth of the particles. However, this reactivity must be investigated more thoroughly before we are able to propose a theory for its precise mechanism.

Band Gap Estimation:

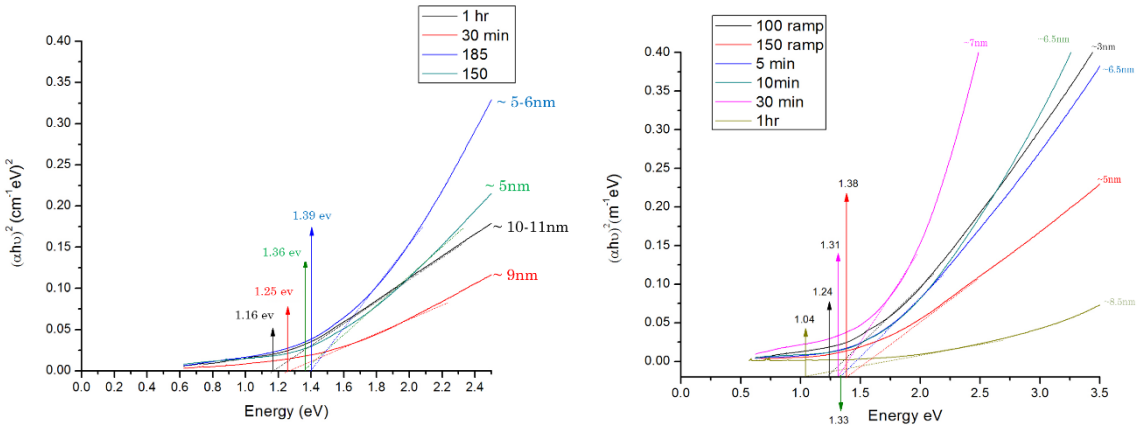

Figure 2.18. *Tauc Plots for band gap estimation for: (left) Kuramite CTS particles formed from heating Cu(I) and Sn(II) (1:1) to 185C showing bandgaps from 1.16eV – 1.39eV; (right) Mohite CTS particles formed from heating Cu(I) and Sn(II) (1:1) to 150 C showing bandgaps from 1.04eV – 1.38eV.*

The effect of the size of a semiconductor nanoparticle on its bandgap is widely known and is useful in developing various optoelectronic devices like thin-film solar cells. **Figure 2.18** (**left**) shows the band gaps of the Kuramite (Cu_3SnS_4) phase CTS particles formed by reacting Cu(I) to Sn(II) in 1:1 ratio at 185°C and (**right**) shows the band gaps of the Mohite (Cu_2SnS_3) phase CTS particles formed by heating the same to 150°C. The data was calculated and is shown in the form of a Tauc plot derived from the UV-Vis absorption data obtained for each sample.

As shown by the **Figure 2.18** (**left**) the band gaps obtained by the Kuramite CTS particles range from 1.16eV to 1.38eV corresponding to 11nm – 5nm particles. This is consistent with the known property of nanoparticles that with decreasing particle size shows an increase in band

gap. Similarly, in **Figure 2.18** (**right**) the band gaps shown by Mohite CTS particles range from 1.04eV to 1.38eV corresponding to particles of sizes 8.5nm to 3nm. In either case the band gaps exhibited by the particles fall within the range of band gaps that are optimal for various photovoltaic applications.

2.5 Further Experimentation and Analysis

The work on Copper Tin Sulphide shown in this chapter, outlines a method for CTS phase separation based on soak temperature and a path towards size focusing of the nanoparticles by increasing the tin concentration. However, this study in by far incomplete and would require more thorough experimentation and characterization to arrive at a solid conclusion. The following outlines a series of further experiments to obtain a better understanding of the science.

1. Broaden temperature series:

The study so far has investigated 2 soak temperatures in the heat up method used to synthesize CTS NPs (150°C and 185°C). These temperatures have suggested the separation of the CTS phases of Kuramite and Mohite. However, to truly understand this phase separation we would be required to soak the NPs at a variety of other temperatures like 50°C, 100°C, 165°C and 200°C. This will not only help in confirming the reproducibility of the Mohite- Kuramite phase separation but also indicate whether or not there are other pure phases obtained when the CTS NPs are soaked at lower or higher temperatures. It may also suggest a transition temperature where one might find a 50-50 phase mixture.

2. Effect of rate of ramp on phase achievement:

The synthesis of CTS used in the study fixed a 20 min ramp to the desired temperature. It is crucial that we experiment with varying ramp rates like (5min, 10 min, 30 min, 1 hour and 2 hour) to ensure that we achieve the phase separation regardless. It is a hypothesis that if the ramp rate is high some phases will cede to form, and slower rates will form increasingly mixed phases. This experiment will help us in understanding the kinetics of phase transformation which we may use further to fine tune this phase separation and obtain purer CTS phases.

3. Cu(II):Sn(IV) experimentation:

The combinations of various Cu and Sn valencies have revealed that reactions with Sn(IV) show a drastic difference in growth rates. The combination of Cu(II) with Sn(IV) however has not been included in the analysis so far. The effect of the valencies suggest the influence of the different valencies of the salts used in the growth rates of the CTS NPs. Based on the observations made from the Cu(I) – Sn(IV) reaction we can hypothesize that Cu(II) with Sn(IV) will result in similar rapid NP growth. Any difference thus that would be observed would shed more light on the exact effect of Sn(IV) and the reaction kinetics that are occurring in the one pot synthesis.

4. More Cu:Sn ratios :

The distinctive size focusing of the CTS nanoparticles to smaller diameters observed due to doubling the Sn ratio to that of Cu hints at a convenient method of NP size control without impacting the CTS phase. However, this study was performed only on 2 Cu:Sn ratios namely 1:1 and 1:2. More permutations would be required for example, 2:1, 1:3, 3:1, 2:3, 3:2 and even 4:1 and 1:4. This will provide a broader picture about the growth rates and NP

sizes obtainable and its impact to the stoichiometry of the CTS particles themselves. It is quite possible that at particular ratios of Cu:Sn the phase may change as well. These experiments would help us understand this delicate balance and help prevent polydispersity and phase impurity.

5. Quantitative analysis on growth rates:

Qualitatively we observed that the Sn ratio and the valencies of the Cu and Sn salts affect the final NP size obtained. As listed in the points before more experimentation is required to exhaustively study the remaining combinations. However, in each experiment we are required to analyze the growth rates to have a more quantitative understanding of the growth mechanism. This is crucial in order to understand not only the growth rates and the influence of the salts but also the nature of the growth model be in Ostwald ripening or Coalescence or other mechanisms. This knowledge will help describe our synthesis method better and also allow us to control the growth of the NPs in situ or as a post synthesis treatment as designed in the earlier $Cu_{2-x}S$ project. This has the impact to contribute significantly to the understanding of ternary nanoparticle growth and methodologies for accurate size focusing and monodispersity.

6. TEM characterization of nanoparticles:

The study of CTS has resulted in some very interesting observations however more material characterization is required to confirm out results. The size analysis for this study was based on the Debye Scherrer method derived from the XRD peaks. In the case of nanoparticles this method of analysis is prone to errors emerging from back ground subtraction and the peak widths themselves. Thus, a better characterization method would be TEM where we

can visualize the particles better and obtain a more reliable particle size and dispersity values. Further, this enables us to observe the morphologies of the CTS NPs and it would be intriguing to note any deviations from the hypothesized spherical shape. Also the various combinations of parameters that have and are yet to be experimented as highlighted in the previous points could possibly show phase purity but with varying morphologies depending on the soak temperature, ramp rate or the tin valency and ratio.

2.6 Conclusion

In conclusion we successfully use the high concentration synthesis in producing phase pure Mohite Copper Tin Sulphide (Cu_2SnS_3) consistently. We showed that the temperature of the soak is of vital importance when tuning the phase as we can easily transition into orthorhombic Kuramite phase (Cu_3SnS_4) if the soak temperature is increased to 185°C while obtaining pure tetragonal Mohite phase at a soak temperature of 150°C. The influence of the Copper to Tin ratio had a remarkable effect revealing that an increase in Tin regardless of its valency result in consistently smaller nanoparticles with a relative reduction in the standard deviation or dispersion in the particle size. This is size focusing is seen repetitively in reaction when Cu:Sn ratios were changed from 1:1 to 1:2 for reactions of Cu(I) with Sn(II), Cu(II) with Sn(II) and most prominently in the reaction of Cu(I) with Sn(IV) showing the largest difference in size deviation (6.5nm to 0.5nm). We hence conclude that an increase in Tin precursor concentration has a size focusing effect on the CTS nanoparticles and plateaus the nanoparticle towards a smaller final size. This seems to imply that the reactivities of Copper and Tin plays an important role in tuning the particle size however the exact nature of this remains to be investigated and quantified. The central achievement of this project was the scalable synthesis approach to high

phase pure CTS nanoparticle with a lowest bandgap of 1.04eV in the Mohite phase and 1.16eV in the Kuramite Phase proving to be quite useful in photovoltaic implementation.

REFERENCES

[1] Global Energy Statistical Yearbook 2017; Enerdata 2009-2018. Retrieved from https://yearbook.enerdata.net/total-energy/world-consumption-statistics.html

[2] Mariusz Malinowski, Jose I. Leon, Haitham Abu-Rub, "Solar Photovoltaic and Thermal Energy Systems: Current Technology and Future Trends", Proceedings of the IEEE, vol. 105, no. 11, pp. 2132-2146, 2017.

[3] Eric O'Shaughnessy, Prog Photovolt Res Appl. 2018;1– 10.

[4] P. Kamat, Quantum dot solar cells. Semiconductor nanocrystals as light harvesters. Journal of Physical Chemistry C, 2008, 112, 18737-18753

[5] D. C. Law, R. R. King, H. Yoon, et al. Future technology pathways of terrestrial III-V multijunction solar cells for concentrator photovoltaic systems Solar Energy Materials and Solar Cells, 2010, 94, 1314-1318.

[6] J. Kolny-Olesiak and H. Weller, ACS Appl. Mater. Interfaces. 2013, 5, 12221.

[7] Claudia Coughlan; Maria Ibáñez; Oleksandr Dobrozhan; Ajay Singh; Andreu Cabot; Kevin M. Ryan. Chem. Rev. 117, 9, 5865-6109

[8] A.C. Lockhande, et al. Chemical Synthesis of Cu2SnS3 (CTS) nanoparticles: A status review, Journal of Alloys and Compounds, 2015, 656, 295-310

[9] Sandra Dias, Kishan Lal Kumawat, Shinjini Biswas, S. B. Krupanidhi; Heat-up synthesis of Cu2SnS3 quantum dots for near infrared photodetection; RSC Adv., 2017, 7, 23301

[10] Sandra Dias, Kishan Lal Kumawat, Shinjini Biswas, S. B. Krupanidhi; Solvothermal Synthesis of Cu_2SnS_3 Quantum Dots and Their Application in Near-Infrared Photodetectors; Inorg. Chem. 56, 4, 2198-2203

[11] Sandra Dias, and S. B. Krupanidhi; Solution processed Cu2SnS3 thin films for visible and infrared photodetector applications; AIP Advances 6, 025217 (2016); doi: 10.1063/1.4942775

[12] Sandra Dias1 and S B Krupanidhi; Cu2SnS3 nanostructures for inorganic–organic hybrid infrared photodetector applications; 2016 Mater. Res. Express 3 105006

[13] DAQING Wu CHARLES R. KNOWLES LUrE L. Y. CHANG; Copper-Tin Sulphides in the system Cu-Sn-S. MINERALOGICAL MAGAZINE, JUNE 1986, VOL. 50, PP. 323-5

[14] Peng, X. G.; Wickham, J.; Alivisatos, A. P. Kinetics of II-VI and III-V Colloidal Semiconductor Nanocrystal Growth: "Focusing" of Size Distributions. J. Am. Chem. Soc. 1998, 120, 5343−5344.

[15] Clark, M. D.; Kumar, S. K.; Owen, J. S.; Chan, E. M. Focusing Nanocrystal Size Distributions via Production Control. Nano Lett. 2011, 11, 1976−1980

[16] C.B. Williamson, D.R. Nevers, T. Hanrath, R.D. Robinson, "The Prodigious Effects of Concentration Intensification on Nanoparticle Synthesis: A High-Quality, Scalable Approach," J. Am. Chem. Soc. 137, 15843 (2015). DOI: 10.1021/jacs.5b10006

[17] D. Kwek, A. Crivoi, and Fei Duan; J. Chem. Eng. Data 2010, 55, 5690–5695

[18] XC Jiang1*, WM Chen1 , CY Chen1,2, SX Xiong1 , AB Yu1; Role of Temperature in the Growth of Silver Nanoparticles Through a Synergetic Reduction Approach; Jiang et al. Nanoscale Res Lett 2011, 6:32

[19] Chem. Commun., 2015, 51, 13810 – (Kuramite 317 orthorhombic peak)

[20] P.A. Fernandes et al. / Journal of Alloys and Compounds 509 (2011) 7600– 7606 – (Mohite – 3 peaks tetragonal)

CHAPTER 3

FUTURE OUTLOOK

Abstract

In this section of the thesis we articulate the future studies that can be pursued based on the work stablished in the previous chapters. Our discoveries and theoretical understandings of scalable nanoparticle synthesis allow us to come up with a few evolutionary ideas that could provide further clarifications to certain unanswered questions or probe further the extent of use for both the particle reusability concept and the scalable CTS nanoparticle synthesis. Firstly, we would like to investigate if we can form a cycle where we constantly grow particles of a size re-etch them and grow them into particles of a drastically different size. Further we would like to answer the question of how polydisperse a particle set can we begin with and how precisely could we tune the sizes of the particles. Next, we would like to investigate if this concept holds just as well with other chalcogenide systems like those of PbS/Se or CdS/Se. Our next proposal is to figure out if we can use the particle reusability to etch and regrow ternary compounds just as easily or is there any new complications due to the presence of a second metal precursor. The last future prospects we suggest is in relation to the actual incorporation into an opto-electronic device to reveal if the monodispersity and phase purity of the nanoparticles achieved truly does provide an improvement in the efficiencies. We appreciate that our results so far have probed but a small distance in nanoscience and there remains a dire need of continued research for sustaining breakthroughs and progress in nanotechnology.

1. Cyclic Etch and Regrow of Nanoparticles:

In Chapter 1 we developed a concept of particle re-usability where a large batch of particles could be separately size tuned with the help of an etchant and heat-up growth in a solution saturated with monomers. We understood how to control the monomer concentrations and in turn tune the dispersity. Our future proposal is to investigate if we can controllably etch and regrow particles repeatedly in a cyclic fashion. The schematic shown in Figure 3.1 illustrates this vision with more clarity.

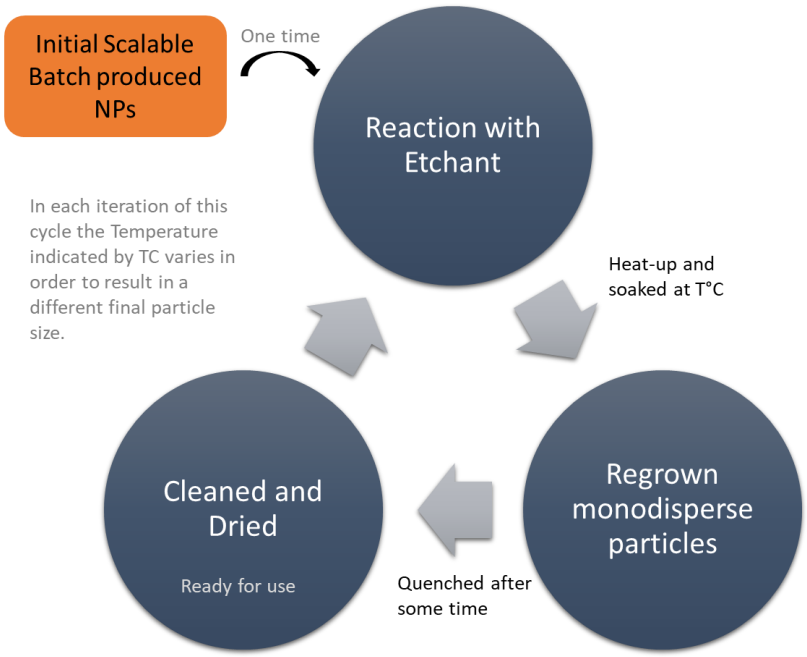

Figure 3.1 A schematic illustrating the process flow of the cyclic reusability of nanoparticles. Here the first batch synthesized nanoparticles are etched and regrown to a particular size and these resultant particles are reused as the batch NPs for another iteration of the cycle differing only in the soak temperature resulting in a set of NPs of a different final size.

Here we start with a batch of nanoparticles produced using the scalable high concentration synthesis method. Then using our post synthesis treatment, we etch the particles and regrow them to a desired size say 8nm. The question we would like to answer here is could we cycle these 8nm particles (after cleaning them) back into the same etch and heat-up procedure and produce size focused 10nm particles? This should be possible by increasing the soak temperature as we have seen that increasing temperature increases the size of the particles without changing the phase of $Cu_{2-x}S$ nanoparticles. Further inspections could be done to find out how large or how small a particle can be made using this method and what are the limitations. Another matter of curiosity is if there are any limitations to the extent of polydispersity in the initial batch of seeds for this etch and regrow method provide robust result consistently. This could be answered by mixing very particles of various sizes with a maximum of 50nm to a minimum of 3nm and observing the particle size and dispersion after the treatment. These studies could greatly increase our understanding of the dynamics of the mechanism as well as quantify the limitations of its use.

2. Expansion of particle reusability to other systems:

Future research corresponding to the regrowth of size focused nanoparticles is to consider implementation of the approach on related chalcogenide systems. The scalable high concentration synthesis procedure previously developed by our group[] was successfully implemented for the production of PbS and CdS nanoparticles. It is curious to find out if the etch and regrowth trend applies to these systems as well.

Positive results would increase the usefulness of the concept and extend its effect in synthesizing not only copper chalcogenides but other related materials like CuSe, PbSe, etc. This could then help in increasing efficiencies for the applications that the CdS and PbS nanoparticles find use.

3. Etch and Regrowth method for size focusing CTS nanoparticles:

In Chapter 2 we discuss the synthesis of phase pure CTS and its various uses. We show that the approach compliments scalable nanomanufacturing. We would now like to explore ways for size tuning the produced CTS nanoparticles. From Chapter 1 we illustrated a convenient mechanism to do so without having synthesize new particles. The question in consideration now is whether we can use this etch and regrowth mechanism to form size focused monodisperse CTS nanoparticles.

The factors that need to be considered are that does OLA have the same etching effect on Tin and hence etch the CTS nanoparticles uniformly or would it selectively etch out one component. Would it change the stoichiometry of the CTS nanoparticle or would it remain phase pure? If the results are positive we could probe further on how small or large the particles could be made. On the other hand, if the stoichiometry does change we could inspect methods on controlling them and quantify vacancy production. Control in vacancies could in turn lead to further investigation on ways to dope the particle and increase electron and hole pair production.

4. Device incorporation of synthesized nanoparticles:

Lastly, we propose the incorporation of the nanoparticles synthesized into a thin film solar cell. Studies need to be done to quantify improvements in the efficiencies and the absorption

coefficients of the materials after phase and size optimization. We could consider various deposition methods and fabrication techniques to optimize device output. Work would need to be done in examining various metal contacts and substrates. Research could be extended to incorporate these thin films onto flexible substrates. As the particles are synthesized in an organic environment they could prove to be very compliant with organic substrates. Furthermore, we could explore different deposition methods that can be incorporated in a roll-to-roll manufacturing of devices. This could in turn have a profound impact in the development of flexible photovoltaics.